

Human-like control for offshore excavators

M. J. Stijnman

Master of Science Thesis



Cover image from: TMS Dredging equipment. <http://www.tms-engineering.nl/documents/dredging-and-shipbuilding/dredging-equipment.xml>

Human-like control for offshore excavators

by

Marco Stijnman

For the double degree of Master of Science in BioMechanical Design & Systems and Control
at Delft University of Technology.

Student number: 4088697

Department : Biomechanical Design
Systems & Control

Project duration: August 1, 2016 – September 12, 2017

Thesis committee:	Dr. Ir. D.A. Abbink	Chairman BMD	BMD, TU Delft
	Dr. Ir. J.W. van Wingerden	Chairman DCSC	DCSC, TU Delft
	Ir. R.J. Kuiper	Daily supervisor	BMD, TU Delft
	Ir. S.P. Mulders	External Member	DCSC, TU Delft

An electronic version of this thesis is available at <http://repository.tudelft.nl/>.

Acknowledgements

During the long journey at the TU Delft I have had the pleasure of being surrounded with many amazing people and I can safely say that without a doubt you all have been the best part of my time here. Way too many people deserve my gratitude, and I would like to thank everyone for supporting me, one way or another, during this time.

I would like to thank David Abbink and Jan-Willem van Wingerden for supervising me during this thesis and whose advice helped me to bring my work to a higher level.

Thanks to Roel Kuiper, who did not only provide daily supervision but much more than that. I will fondly remember the many conversations we had over equally as many coffees, all the advice you gave me, your critical thinking and enthusiasm, and last but not least all the laughter we shared.

Many thanks to SeaTools and all its employees, who welcomed me to work part-time on my thesis at their company located in Numansdorp, the Netherlands, where I received indispensable aid in the form of knowledge, software and hardware, various great barbeques and an endless supply of fruit.

Thanks to my family, who have always supported and motivated me yet gave me the freedom to make my own choices. To my father and mother, the most kind-hearted and loving parents a son could wish for. To my sister and her family, for leading the way. To my brother, for being the most pure definition of happiness and joy.

Thanks to Gaia, for always believing in me, even in times in which I doubted myself. You always pulled me out of it and brightened my days. We've had many experiences and adventures, and I am looking forward to sharing many more with you, wherever we end up going.

Finally, thanks to all my friends. Whether you lived, partied, drank, dined, climbed, gamed, or studied with me, you've been an irreplaceable part of this. Thank you, everybody.

Preface

This thesis report is submitted in order to fulfil the requirements for the Double Degree of Master of Science for the departments of BioMechanical Design and Systems & Control at the Technical University of Delft, the Netherlands. Supervision was provided over the entire duration of the thesis by dr. ir. D. A. Abbink, dr. ir. J.W. van Wingerden, and ir. R.J. Kuiper.

Marco Stijnman
4088697
Delft University of Technology
12th September, 2017

Contents

I Introduction	2	V Conclusions and future work	19
I-A Human-centered automation: towards human-like control	2	References	20
I-B Model Predictive Control	3	Appendix A: Additional modelling explanations	21
I-C Extension to Adaptive Model Predictive Control	4	A-A Hydraulic equations	21
I-D Thesis objective	4	A-B Soil memory block	21
II Excavator model	4	A-C Water drag forces	21
II-A Kinematics and dynamics	4	Appendix B: MPC problem setup elaboration	22
II-B Hydraulics	5	B-A Prediction matrices	22
II-B1 Hydraulic valves	5	B-B Translating the cost function to the standard QP format	23
II-B2 Hydraulic cylinders	5	Appendix C: Familiarization stage tasks	24
II-C Soil interaction	6	Appendix D: Learning curves	25
II-D Excavator model evaluation	6	Appendix E: Determination of the input smoothness metric SD and the performance metric RMSE	27
II-E Sub-conclusions on the excavator model	7	Appendix F: Extra figures: comparisons for task B1 and B2, input reversals	29
III Adaptive Model Predictive Control	7	Appendix G: Performance of Subject 6 for task A	33
III-A Internal model	7	Appendix H: Frequency response plots	34
III-B Online parameter estimation with an Extended Kalman Filter	8	Appendix I	35
III-B1 EKF description	9		
III-B2 EKF evaluation	9		
III-C Model Predictive Control implementation	10		
III-D Simulation task setup	11		
III-E Simulation task results	11		
III-E1 Situation 1	11		
III-E2 Situation 2	12		
III-E3 Situation 3	12		
III-F Discussion on the Model Predictive Controller	13		
III-G Sub-conclusions on the Model Predictive Controller	13		
IV Human factors experiment	13		
IV-A Method	14		
IV-A1 Participants	14		
IV-A2 Apparatus	14		
IV-A3 Experimental design	14		
IV-A4 Dependent measures	15		
IV-B Results	16		
IV-B1 Similarity in task A	16		
IV-B2 Performance	17		
IV-C Discussion on the human factors experiment	18		
IV-C1 Similarity	18		
IV-C2 Performance	18		
IV-D Sub-conclusions on the human factors experiment	19		

Human-like control for offshore excavators

Marco Stijnman, Roel Kuiper, Jan-Willem van Wingerden, and David Abbink

Abstract—Offshore excavators are large hydraulically driven machines which are difficult to control due to slow dynamics, inherent nonlinearities, a varying environment and complex kinematics. As digging is performed under water, only limited visual feedback of the task can be provided by means of a visualization interface. Operators require an extensive amount of practice before being capable of achieving sufficient and consistent performance. Often, automation is implemented as a way of reducing costs related to expensive operators and attaining consistent performance. However, automation struggles with adapting to unforeseen situations and a large task variety, which are areas human operators excel in. Instead of attempting to fully automate excavators, this thesis takes a more human-centered approach, and focuses on the design and evaluation of a human-like controller to *partially* automate excavator operations, while assuming a human operator is still present to trade or share control with. In order to simultaneously deal with the various nonlinearities in the system while providing human-like control this work proposes the use of an Adaptive Model Predictive Controller, whose underlying principles are similar to those of humans.

To determine whether the controller is indeed human-like a complex excavator model including a realistic soil model was developed and used to implement and tune the controller. Finally, a simulator experiment was conducted to compare the subjects and the controller in terms of performance for various tasks and the control behavior similarity for a well-trained task. Eight subjects controlled the excavator model and performed four stages, starting with a familiarization stage in which the subject got accustomed to the system. The other three stages (easy, difficult, boulder) featured a 9 m long target path, with conditions of varying difficulty between stages. The controller showed 2 to 3 times lower tracking errors for both the easy and difficult stage while providing 1.5 to 5 times smoother inputs, but could not overcome the unforeseen boulder whereas all subjects could, showcasing the importance of having humans and automation complement each other. Furthermore, a high quality fit (VAF > 70%) was found between the boom inputs of the subjects and the controller in the well-trained easy stage, indicating human-like control.

Index Terms—Offshore excavator, adaptive model predictive control, extended kalman filter, human-like control

D.A. Abbink and R.J. Kuiper are with the Cognitive Robotics Department and J.W. van Wingerden is with the Delft Center for Systems & Control, Faculty of 3mE, Delft University of Technology, Mekelweg 2, 2628 CD Delft, The Netherlands.

I. INTRODUCTION

IN today's world defined by speed and slim cost margins automation is a hot topic. This is no different for the dredging industry, which uses offshore excavators in order to remove soil below the water's surface. The demand for automation arises due to the difficulty of controlling these excavators. Offshore excavators are characterized by slow dynamics, inherent nonlinearities, a varying environment, and complex kinematics [1]. As digging is performed under water, only limited visual feedback of the task can be provided by means of a visualization interface [2]. Furthermore, incorrect control can damage the machine, increasing maintenance costs. As such, only well-trained and thus expensive operators are capable of attaining sufficient and consistent performance.

Resolving these issues by automating these complex machines continues to pose severe challenges [3]. Offshore excavators are located in environments in which unforeseen disturbances can always occur, and it is not always economically or physically possible to monitor everything using sensors. Furthermore, these excavators perform a variety of tasks which all require in-depth knowledge, which is difficult to capture in robust control algorithms. Human operators are much better than control algorithms at learning a large variety of tasks and adapting to these unforeseen situations.

Instead of attempting to fully automate excavators, this thesis takes a more human-centered approach, and focuses on the design and evaluation of a human-like controller to *partially* automate excavator operations, while assuming a human operator is still present to trade or share control with.

A. Human-centered automation: towards human-like control

The interaction between man and machine has been examined for decades and various human-factors scientists have since then reiterated that the binary "either man or machine" approach is unproductive [4] [5], and that more interaction between both man and machine is necessary. This principle is adopted in human-centered automation [6]. Essentially, this concept states that humans and automation should understand each other's intents,

and that system designers should attempt to automate systems with this idea in the back of their minds, as opposed to technology-centered automation in which the human is essentially expected to handle whatever the system designers did not manage to automate, without much regard for the operator’s desires. By keeping the human in the loop and informed about the automation at all times, issues such as overreliance, loss of situational awareness, complacency, and increased mental workload, which eventually lead to distrust/disuse [7]–[9] can be avoided or alleviated. This design philosophy holds regardless of the type of partial automation, whether it be supervisory control [10] or shared control [11]; situations in which the operator is uncertain about what the system does or wants should be avoided.

However, especially in systems where both controller and human share control and continuously work together conflicts may occur. This phenomenon is reported in various studies such as [12]–[14] and can have various origins, such as the existence of differences in the control strategy, control objective, or underlying control structure of the human and the controller. A mismatch in either one can mean the controller and operator do not agree on the desired input to the system, leading to increased control effort and mental workload and, if mismatches persist, ultimately distrust/disuse. Designing a more human-like controller using a human-centered approach is therefore hypothesized to lead to a reduction in the amount of conflicts [6].

An understanding of how humans control systems, and hence an understanding on how to obtain a more human-like controller, can be obtained from research performed in the field of neuroscience. It has been shown that humans create internal models when interacting with systems, which are then stored in the cerebellum [15] [16]. Upon interacting with a system for which an internal model is present this model is recalled and used to predict the behavior of this system. This enables the central nervous system to utilize feed-forward control, instead of having to only rely on feedback mechanisms.

Furthermore, humans do not only aim to minimize the output error of the task they are performing, but also take the amount of input effort they have to provide to the system into consideration [17] [18]. This has effects for the desired functionality of the controller; achieving excellent reference tracking is meaningless if the input varies wildly and is perceived as annoying by the operator.

A control method that includes an internal model and input weighting is thus likely to be a suitable method for human-like control. One such method that contains both of these characteristics is Model Predictive Control

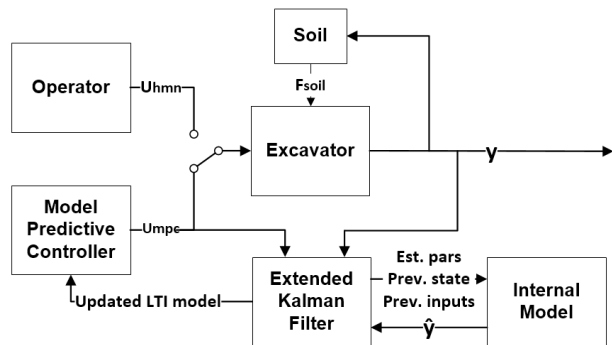


Fig. 1: Block scheme of the control loop of the excavator. The standard MPC is extended with the Extended Kalman Filter and the internal model, used for parameter adaptation.

(MPC), and an example of how both the operator and MPC could be combined in the same control loop is shown in Fig. 1. The switch indicates that the operator and the MPC are evaluated separately in this study, but could be replaced by a haptic interface [19] in future work to enable shared control.

B. Model Predictive Control

Model Predictive Control is an advanced control technique that incorporates an internal model in order to predict the future behavior of the system, enabling feedforward control [20]. Furthermore, by using weights in the cost function emphasis can be shifted between performance and control effort. This is essentially exactly what human operators also do, making it a very suitable method for human-like control.

Purely from the excavator’s perspective, MPC is also a well suited control technique. The excavator uses its joystick inputs to open or close hydraulic valves which naturally cannot exceed their physical limits. This introduces input constraints into the system. A major advantage which MPC has is the possibility of incorporating constraints on the input, input rate of change, state, or output, in contrast to simpler control methods such as Linear-Quadratic Regulators (LQR) or Proportional-Integral-Derivative (PID) controllers. These constraints are taken into account *during* the optimization step of the cost function, whereas other control methods calculate the control inputs as if there were no constraints at all. Furthermore, the possibility of tuning the trade-off between input smoothness and performance is also important for the system: frequent switching wears out the large hydraulic valves faster, requiring costly maintenance.

However, in addition to being human-like the MPC must also be capable of controlling the complex excavator. This aspect requires an extension of the MPC algorithm, as standard MPC is not capable of accounting for the various nonlinearities existent in the excavator.

C. Extension to Adaptive Model Predictive Control

While MPC is suitable for human-like control and can incorporate input constraints, standard MPC only uses a Linear Time Invariant (LTI) model of the excavator. However, several nonlinear characteristics of the excavator cause a change in the behavior of the excavator which should be reflected in the LTI model. Firstly, the inertia perceived by the boom arm depends on the extension of the stick, creating a coupled effect between the two arms. Secondly, the behavior of the hydraulic cylinders driving the arms is direction dependent due to differences between the piston-side and rod-side of the cylinders. As a result, upwards motions are slower than downwards motions. Finally, the transition between water and soil drives a change in dynamics, and within the soil fluctuations in soil strength can always appear and are not a priori known.

The issue of incorporating these nonlinear characteristics can be resolved by extending standard MPC with online adaptation by using an Extended Kalman Filter (EKF) [21]. The EKF utilizes a simplified, nonlinear internal model in order to construct a one-step-ahead prediction of the system. The predicted output is then compared to the actual output to obtain the prediction error. The parameters of this nonlinear internal model are then adapted based on the prediction error in order to converge the prediction to the real output. Afterwards, a linearized version of this nonlinear model is passed to the MPC. In this manner the MPC is provided with an accurate LTI model suited for the current situation of the excavator, enabling accurate predictions while still allowing the use of relatively simple control algorithms. The total control loop, consisting of the operator, the excavator including its soil model, and the Adaptive MPC can be seen in Fig. 1.

D. Thesis objective

Summarizing, it is hypothesized that Adaptive Model Predictive Control can provide human-like guidance for a complex excavator model by providing similar control inputs as human operators, while attaining low tracking errors. In order to validate this hypothesis several problems will be tackled during this thesis. First of all, a complex excavator model is constructed which serves as the system both the controller and the human operators

will control. Secondly, an adaptive MPC is designed and evaluated for various test cases. Thirdly, a human factors evaluation is performed in order to compare the controller to the operator. Finally, the work is concluded and the direction of future work is outlined.

II. EXCAVATOR MODEL

A complex excavator model must first be developed as the system which will be controlled by both the controller and the human operators. This excavator model consists of three major components. These are the mechanical system, the hydraulic system, and the interaction with the soil. The inclusion of a hydraulic system not only introduces the disparity between upwards and downwards motions, but also enforces input constraints to be taken into account. Previous studies instead applied the control input directly to the joint, circumventing these issues [22] [23]. Studies that do include the hydraulic system instead completely leave the soil out of their scope [24]–[26].

A simplified drawing of the mechanical system of an excavator from which the necessary dynamics and kinematics can be derived is shown in Fig. 2, showcasing the four linkages: the base, boom, stick and bucket. These arms are brought into motion by the hydraulic system, which translates the inputs given by the user to forces on the joints of the excavator. Finally, the soil interaction describes the forces that are applied on the excavator as a result of moving through the soil.

A. Kinematics and dynamics

The forward kinematic equations are used to determine the position of the endpoint (the tip of the bucket) for known angles of the arms which are necessary for the construction of the excavator model. Similarly, the inverse kinematics are used to determine the required link angles based on the desired trajectory

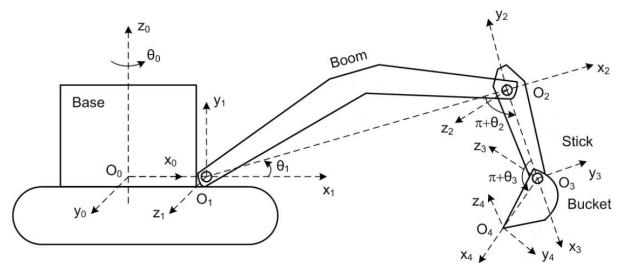


Fig. 2: Simplified schematic drawing of a typical excavator, together with its local coordinate systems and angle definitions. [22].

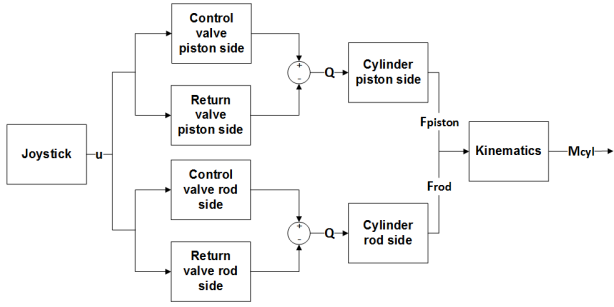


Fig. 3: Schematic overview of a hydraulic cylinder.

of the endpoint. These angles can then be used as the reference trajectory for the controller. The derivations of these equations have been documented in work such as [27].

The excavator dynamics relate the moments applied to the joints to movement and can be described with the equations of motion as listed in Eq. (1):

$$M(\theta)\ddot{\theta} + C(\theta, \dot{\theta})\dot{\theta} + D(\dot{\theta}) + G(\theta) = Q_h(u, \theta, t) - Q_s(\theta, \dot{\theta}, t) \quad (1)$$

where $\theta = [\theta_0 \ \theta_1 \ \theta_2 \ \theta_3]^T$ as defined in Fig. 2, where the subscript indicates the angle of joint i . The input moments originating from the hydraulics are $Q_h(u, \theta, t)$, and the moments resulting from the soil interaction are reflected with $Q_s(\theta, \dot{\theta}, t)$. $M(\theta)$ is the inertial matrix, $C(\theta, \dot{\theta})$ contains the terms due to the Coriolis and centripetal effects, $D(\dot{\theta})$ contains the terms due to friction, and $G(\theta)$ contains the terms due to gravity.

The derivations and full expressions for the matrices $M(\theta)$, $C(\theta, \dot{\theta})$, $D(\dot{\theta})$, and $G(\theta)$ have been well documented in work such as [28] and [23]. Finally, during this study only the digging motion in a 2D plane is considered and thus rotations of the base will not be taken into account.

B. Hydraulics

In Fig. 3 a schematic overview of a hydraulic cylinder is shown, and its implementation will concisely be explained here.

1) *Hydraulic valves*: By operating a joystick the operator provides an input to a directional valve. Based on the direction of the input, this valve either allows flow from the pump into the piston side of the cylinder and flow from the rod side into the tank, or flow into the rod side of the cylinder and flow from the piston side into the tank. The area A which the flow can inhabit ranges from 0% to 100% of the total area of the valve, corresponding to the magnitude of the input signal. An

important point to consider is that valves have a small amount of overlapping area, which means a dead-band phenomenon is present whenever a valve initially starts opening up. The pump and tank are considered as a constant source and sink of 300 and 0 bar, respectively. The flow through a valve is represented as an orifice flow:

$$Q = C_d A \sqrt{\frac{2\Delta p}{\rho}} \quad (2)$$

where C_d is the discharge coefficient, A is the area of the valve, Δp is the pressure difference over the valve, and ρ is the density of the hydraulic fluid.

2) *Hydraulic cylinders*: Essentially, these hydraulic cylinders function as large springs, where the bulk modulus B_m of the hydraulic oil represents the stiffness of the spring. This is part of the reason why controlling these large excavators is so difficult; the operator does not directly apply a moment on the excavator's joints, but instead can only compress or decompress these hydraulic springs. Moreover, another difficulty between the input/output relation originates from the behavior of these hydraulic cylinders. Due to volumetric differences between the piston-side and the rod-side of the cylinders, upwards motions are slower than downwards motions.

The cylinders of the excavator are all double-acting cylinders. The pressure generated in each side of the cylinder can be calculated based on the bulk modulus:

$$P = B_m \frac{V - V_0}{V_0} \quad (3)$$

Where for each side P is the pressure in the respective side of the cylinder, B_m is the bulk modulus of the hydraulic oil, V_0 is the initial cylinder volume per side for the current configuration and V is the volume of the hydraulic oil residing in the respective side. The flow Q , obtained from the proportional valve and calculated in the previous section, is integrated over time to calculate V . This means that for every simulation step, for each side of the cylinder, the initial volume is calculated based on the position of the links of the excavator and thus the extension of the rod. Then, any incoming or outgoing flow is added to or subtracted from the current volume. Increasing the amount of hydraulic oil while not proportionally increasing the available space it can inhabit will cause an increase in pressure, based on the bulk modulus of the fluid. The total force exerted by the rod can then be calculated:

$$F = P_{ps}A_{ps} - P_{rs}A_{rs} \quad (4)$$

where the subscripts ps and rs indicate the piston side and rod side, respectively.

Lastly, the kinematic equations necessary to relate the force generated by the cylinder to the moment Q_h it exerts on its respective joint are very excavator specific. The attachment point of the rod and the configuration of the supporting linkage structure varies between different types of excavators, and can be determined as a function of a series of trigonometric equations. This same process can be applied for other joystick inputs controlling different valves and cylinders, resulting in the hydraulically generated torques on all the excavator's joints.

C. Soil interaction

The forces resulting from the interaction with the soil are based on the sand force model of [29]. This paper provides formulas for the amount of force required to penetrate different types of soil dependent on for instance soil hardness, the cutting angle and the cutting depth.

The application of the forces on the excavator is done by modelling three virtual spring-damper systems located between the bucket and soil which is in contact with the bucket, as depicted in Fig. 4.

During normal digging motion, the bucket applies force on the forwards and downwards springs and compresses them until they reach the amount of force required to penetrate the soil. The springs then remain compressed and move along with the tip of the bucket, while exerting their maximum force on the bucket. When the bucket reverses or leaves the soil, the springs are decompressed. Furthermore damping is present, limiting the velocity with which the bucket can move. The combination of stiffness and damping provides a realistic approach at modelling the soil interaction while still being fairly simple.

In the backwards direction the spring/damper system is much stronger, and only allows a limited amount of movement. Furthermore the vertical spring provides greater resistance when the bucket is attempting to dig with an angle that is more than 45 degrees with the horizontal. Both of these additions ensure realistic digging by limiting digging motion misaligned with the teeth.

D. Excavator model evaluation

In order to evaluate the model several characteristics are reported in Table I and Table II, presenting an idea of the behavior of the excavator. As seen in the Table II, the position of the stick indeed has an influence on the dynamics of the boom, significantly impacting the time taken for a movement over the full range of motion.

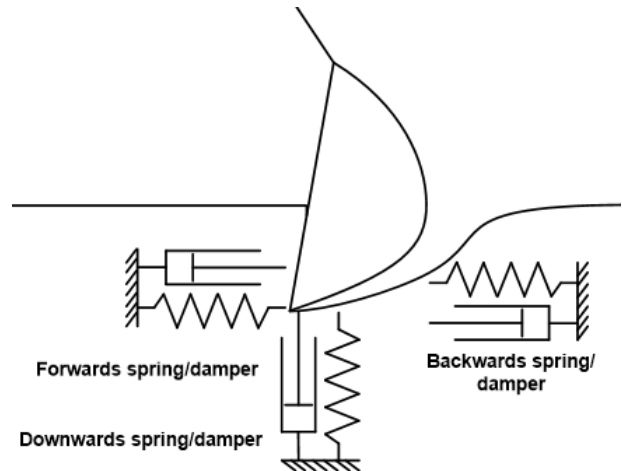


Fig. 4: Schematic drawing of the interaction between bucket and soil. Although drawn at different positions for clarity, all forces are applied at the tip of the bucket.

TABLE I: Length, weight and range of motions of the three arms of the excavator.

	Boom	Stick	Bucket
Length [m]	12.0	7.0	2.3
Weight [kg x 1000]	14.1	7.1	4.6
Range of motion [deg]	-46 to 62	-148 to -34	-99 to 50

This effect is visualized in Fig. 5, where, for a part of the range of motion, the movement of the boom is shown for various positions of the stick while the same input is applied in all three cases.

Furthermore, Table II shows a large difference in the movement durations between an upward and downward motion. This effect is indeed reflected in Fig. 6, in which the response of the boom as a result of two step inputs in opposite directions are shown. The disparity between downwards and upwards motions is clearly noticeable: the angular velocity in downwards direction is more than

TABLE II: Movement durations in which the boom or stick are provided with a maximum joystick input. The reported times represent the time it took to cover the full range of motion for the boom and the stick. Note that since the position of the stick affects the dynamics of the boom, two situations are reported: Stick Expanded (S.E) and Stick Retracted (S.R).

Movement duration [s]			
Boom		Stick	
Up	Down	Left	Right
45.1 (S.E)	16.2 (S.E)	13.5	14.2
35.9 (S.R)	18.0 (S.R)		

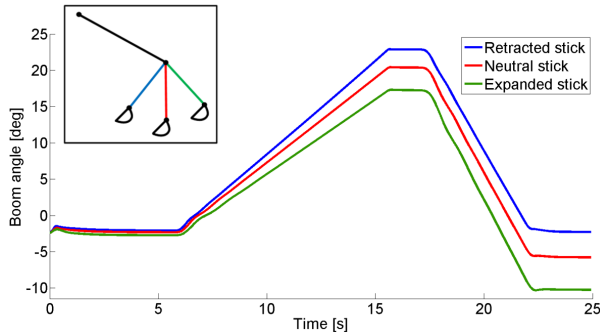


Fig. 5: Non-linear effect of the stick position on the boom dynamics. While the same input sequence (an upwards movement followed by a downwards movement) is applied to the boom in all three cases, its output angle varies depending on the extension of the stick. The three stick positions are indicated in the top-left image.

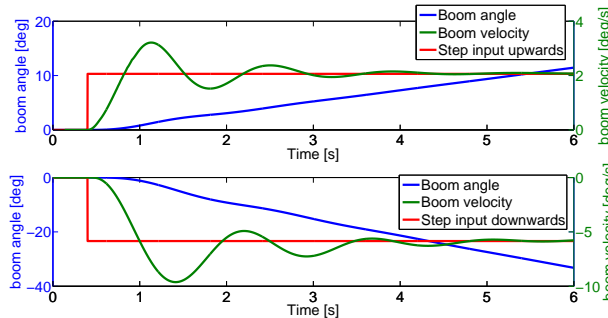


Fig. 6: Step responses of the boom for step responses in upwards (upper subplot) and downwards (bottom subplot) direction. The stick was fully extended in both cases.

2.5 times as high as in the upwards direction. This figure also highlights the fact that the excavator is controlled using rate control, in which the inputs of the joystick correspond to the angular velocity of their related arms.

E. Sub-conclusions on the excavator model

The excavator model constructed in this section exhibits relevant and realistic (nonlinear) behavior in simulations, and was partially based on [23], whose descriptive work on the dynamic model for excavators is commonly used as a basis for other studies related to excavators. In this thesis this dynamic model is extended with a hydraulic system and a soil model, which includes realistic spring-damper behavior extended from the work of [29].

Previously performed studies lack either the inclusion of a hydraulic system or a realistic soil model. Both

of these components have consequential effects for the dynamics of the system and thus for the determination of a control method for the system, creating the need for a controller capable of dealing with a varying environment without having a priori knowledge.

III. ADAPTIVE MODEL PREDICTIVE CONTROL

Model Predictive Control (MPC) is an advanced control technique that incorporates an internal model in order to predict the future behavior of the system, enabling feedforward control. Furthermore, by using weights in the cost function emphasis can be shifted between performance and control effort. This is essentially exactly what human operators also do, making it a very suitable method for human-like control. In this thesis standard MPC is extended using an Extended Kalman Filter (EKF) in order to allow online adaptation.

In this section the internal model is first constructed, followed by the implementation of the EKF. Then, the implementation of the MPC algorithm is described and finally evaluated for various scenarios.

A. Internal model

Due to the complexity and size of the excavator model a simplified model must be created. This step is necessary for the MPC since it predicts and optimizes the system's behavior over a certain amount of time at each controller interval. An increase in internal model complexity thus goes hand in hand with a large increase in computational power demand.

In order to simplify the control aspect of this thesis for both controller and human operators the bucket angle is internally controlled using a simple P controller. The bucket angle while cutting is generally kept around 45 degrees and since the dynamics of the bucket, which is a lot smaller than the boom or the stick, are much simpler a P controller is easily able to keep the bucket at the desired angle. This leaves a two input/two output system, having the boom and stick joystick commands as input, and the boom and stick angles as output.

The simplified internal model was set up as shown in Fig. 7 from which its equations of motion can be derived using Euler-Lagrange equations. The two angles θ_1 and θ_2 were taken as the generalized coordinates q_1 and q_2 , corresponding to the boom and stick angle. Then, defining $q = [q_1 \ q_2]^T$, the mapping of the coordinates of the center of masses of both links $r(x, z, \theta) =$

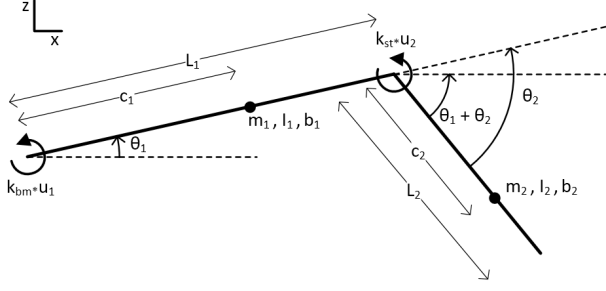


Fig. 7: Schematic drawing of the simplified two-link model used for the internal model.

$[x_{c_1}, z_{c_1}, \theta_1, x_{c_2}, z_{c_2}, \theta_1 + \theta_2]^T$ from workspace to generalized coordinates gives:

$$r = [\cos(q_1)c_1, \sin(q_1)c_1, q_1, \cos(q_1)L_1 + \cos(q_1 + q_2)c_2, \sin(q_1)L_1 + \sin(q_1 + q_2)c_2, q_1 + q_2]^T \quad (5)$$

By defining the mass matrix M_i as $diag(m_1, m_1, I_1, m_2, m_2, I_2)$ the kinetic energy T , potential energy V and Rayleigh dissipation function D_r can be calculated as:

$$T = 0.5 \frac{\partial r^T}{\partial q} M_i \frac{\partial r}{\partial q} \quad (6)$$

$$V = r(2)m_1g + r(5)m_2g \quad (7)$$

$$D_r = 0.5(b_1\dot{q}_1^2 + b_2\dot{q}_2^2) \quad (8)$$

Where b_1 and b_2 are the damping coefficients and \dot{q}_1 and \dot{q}_2 are the derivatives with respect to time of the generalized coordinates q_1 and q_2 . By defining the Lagrangian $L = T - V$ the equations of motion can be determined using Lagrangian mechanics:

$$\frac{d}{dt} \frac{\partial L}{\partial \dot{q}} - \frac{\partial L}{\partial q} + \frac{\partial D_r}{\partial \dot{q}} = Q_{im} \quad (9)$$

This Euler-Lagrange equation can be translated into the form of Eq. (1) by defining

$$\begin{aligned} M_{im}(q) &= \frac{\partial \frac{\partial T}{\partial \dot{q}}}{\partial \dot{q}} & C_{im}(q, \dot{q}) &= \frac{\partial \frac{\partial T}{\partial \dot{q}}}{\partial q} \\ G_{im}(q) &= -\frac{\partial T}{\partial q} + \frac{\partial V}{\partial q} & D_{im}(\dot{q}) &= \frac{\partial D_r}{\partial \dot{q}} \\ Q_{im} &= diag(k_{bm}u_1, -k_{st}u_2) \end{aligned} \quad (10)$$

where k_{bm} and k_{st} are the input gains and u_1 and u_2 are the inputs produced by the joysticks for the boom and stick, respectively. The desired angular accelerations can then be determined from the equations of motion:

$$\ddot{q} = M_{im}^{-1}(q)(-C_{im}(q, \dot{q})\dot{q} - D_{im}(\dot{q}) - G_{im}(q) + Q_{im}) \quad (11)$$

and are then discretized using a zero-order hold with a sampling frequency of 500 Hz to match the sampling frequency of the simulated complex excavator.

Note that in order for the simplified model to mimic the characteristic behavior of the excavator the effect of the potential energy V was removed. The pressure built up in the excavator's hydraulic cylinders keeps the excavator stable at any point in the workspace even when no inputs are applied, counteracting the effect of gravity. To avoid the arms of the simplified model simply falling down when no inputs are provided the effect of the potential energy needs to be compensated for by a term of equal magnitude but an opposite sign, which is essentially the same as removing the potential energy altogether.

The constructed internal model is a much more compact model than the complex excavator, but can in its current state not always accurately reflect the behavior of the excavator due to its varying dynamics. The EKF will be used to account for these variations.

B. Online parameter estimation with an Extended Kalman Filter

It is clear that the simplified model presented in the previous section is not yet ready to be handed over to an MPC. Firstly, in this thesis linear MPC is used as nonlinear MPC is much more computationally intensive, while real-time applicability is desired. The nonlinear effect which the position of the stick has on the inertia of the boom as shown in Fig. 5 is still present in the equations of motion in Eq. (11), which means the simplified model will need to be linearized.

Furthermore, the necessity of removing any terms related to soil interaction and the hydraulic system in order to obtain a simple linear model demand additional attention. One approach to deal with nonlinearities resulting from the hydraulic system is system identification on sets of input-output data such as in [25], however in this work soil contact is left outside of the scope. The issue with any techniques solely relying on a priori information is their incapability of incorporating new information. The first major issue is the fact that soil is removed during digging operation. This means that two subsequent identical motions will experience vastly different interaction forces, as the first scoop already removed the soil on this position. The second issue is that soil properties are not known beforehand, and can vary during the digging trajectory.

The approach used in this study is to let the input gains k_{bm} and k_{st} capture these effects by utilizing online adaptation. The EKF approach as described in e.g. [30] and [21] and shown in Eq. (12) is a very suitable candidate for this study, as it utilizes the already constructed internal model for its algorithm. Note that during this study full state information is assumed, alleviating the need for a state observer. However, if necessary, this could be implemented by extending the EKF to a Dual Extended Kalman Filter (DEKF), where two separate Kalman filters are used for both state and parameter estimation.

1) *EKF description*: The full EKF algorithm is shown in Eq. (12) and can be split up in five major steps. For clarity reasons the notations of time are shown in the subscripts.

Time update:

$$\hat{\theta}_k^- = \hat{\theta}_{k-1}^+ \quad (12a)$$

$$\Sigma_{\theta,k}^- = \Sigma_{\theta,k-1}^- \quad (12b)$$

$$\hat{y}_k = f(x_{k-1}, u_{k-1}, \hat{\theta}_k^-) \quad (12c)$$

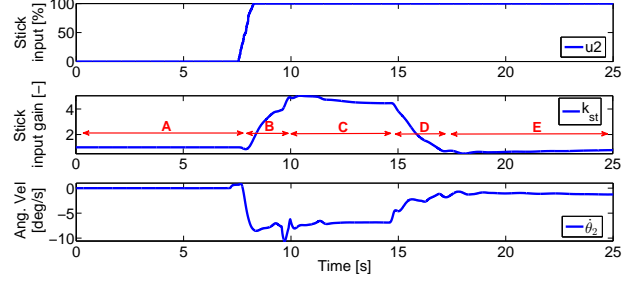
Measurement update:

$$K_k^\theta = \Sigma_{\theta,k}^- (C_k^\theta)^T [C_k^\theta \Sigma_{\theta,k}^- (C_k^\theta)^T + \Sigma_e]^{-1} \quad (12d)$$

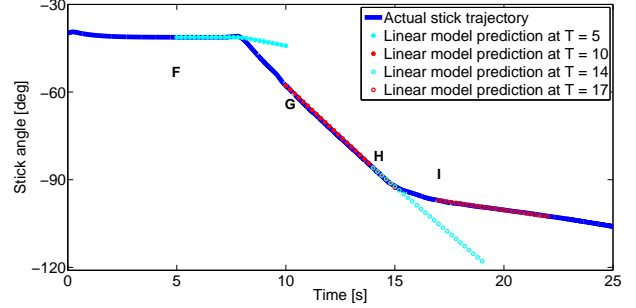
$$\hat{\theta}_k^+ = \hat{\theta}_k^- + K_k^\theta [y_k - \hat{y}_k] \quad (12e)$$

Initially, the parameter estimate and its uncertainty are set to the best a priori guess. In Eq. (12a) and Eq. (12b) the previous timestep's parameter estimate and uncertainty are propagated. By using the state, input, and estimated parameters at time $k - 1$, in Eq. (12c) the simplified model of Section III-A is then used to predict the output at time k .

The Kalman gain in Eq. (12d) contains the term C_k^θ which can be understood as the effect a change in one of the parameters has on the output. This essentially serves as the sensitivity of the parameter, and gives the algorithm the knowledge needed to know whether to increase or decrease the parameter, and how much effect a change has. This term is derived by taking the Jacobian of the nonlinear system w.r.t the parameters of interest. Furthermore, the lower the measurement uncertainty Σ_e the higher the kalman gain. In Eq. (12e) the new parameters are determined using the previous parameters, the Kalman gain and the error between the estimated output and the real output. Note that while in the more common approach the parameter uncertainty would be reduced during the measurement step, in this study it is kept constant as there is no "true" value the parameters converge to, since the parameters are continually changing.



(a) Adaptation of the input gain of the stick during digging. A: Initial situation. B: Excavator enters very soft soil, and the gain is increased. C: Excavator continues digging in the soft soil, gain remains fairly constant. D: Excavator encounters soil with gradually increasing strength, and gain is decreased. E: Excavator continues digging in hard soil, gain remains fairly constant.



(b) Actual stick output and four 5-seconds-ahead predictions of the internal model, made at various points.

Fig. 8: Online adaptation of the stick input gain due to the EKF (upper figure) and predictions of the internal model compared to the real output (bottom figure). Predictions F and H result in deviations from the real output, which the EKF resolves by updating the input gains, resulting in accurate predictions G and I.

2) *EKF evaluation*: In order to validate the internal model and the online estimation its predicted outputs can be compared with the outputs of the complex excavator model. Note that no controller is present here, and a predetermined input sequence is provided to both the excavator and the internal model. Fig. 8 shows a situation in which the excavator boom is kept still and the stick is moved through the soil. The soil profile used is initially very soft, but becomes much stronger after a few meters.

Using the denotation indicated in the middle subplot, Fig. 8a shows that during A the system is initialized. At the start of B the stick input is increased to 100% and the stick enters the very soft soil, and continues digging during C. At the start of D the harder patch of soil is encountered, and digging is continued in the hard soil during E. These situations cause the input gain k_{st} to

adapt itself to fit the internal model to the actual situation. The actual output is indicated by the solid blue line in Fig. 8b, and for reasons of clarity only four 5-seconds-ahead predictions are shown. Prediction **F** attempts to predict the motion of the stick, but its input gain is too low to accurately reflect the situation. However, the EKF adapts to the very soft soil by increasing the input gain during **B**, and as a result prediction **G** matches the output of the excavator. Similarly, at $T = 15$ seconds the stronger soil is encountered, leading to more resistance and thus a reduction in angular velocity, even though the input is kept at its maximum. As seen by predictions **H** and **I**, the model accounts for the change in soil strength by adapting the input gain during **D**, correcting the prediction error.

This approach adapts the input gains of the nonlinear internal model to create a better approximation of the current situation. Subsequently, the model is linearized around its the current state and passed onwards to the MPC.

C. Model Predictive Control implementation

The linearized internal model passed to the MPC by the EKF can now be used to predict the future outputs of the system. These predictions are shown in Eqs. (13) and (14), and their derivation is elaborated upon in Appendix B-A. Note that the model is transformed into an Incremental Input Output (IIO) representation, which results in the optimization of Δu instead of u , allowing the penalization of the input rate instead of the input magnitude. Furthermore, since the internal model is linearized at every control interval, $x(k)$ is always equal to the trim state \bar{x} . This means the term $M(x(k) - \bar{x})$ is always equal to 0. Using a controller sampling frequency of 5 Hz, a value of $N = 20$ was chosen for the prediction horizon, corresponding to a look-ahead time of 4 seconds. Finally, the output at the trimmed position \bar{y} and the previous input $\mathbf{u}(k-1)$ are stacked vectors of length N , indicated by an emboldened symbol. The predictions are:

$$\hat{y}_p = \bar{\mathbf{y}} + M(x(k) - \bar{x}) + \Phi_1 \Delta u + \Phi_2 \mathbf{u}(k-1) \quad (13)$$

Where

$$\hat{y}_p = \begin{bmatrix} \hat{y}_p(k+1) \\ \hat{y}_p(k+2) \\ \vdots \\ \hat{y}_p(k+N) \end{bmatrix} \quad \Delta u = \begin{bmatrix} \Delta u(k) \\ \Delta u(k+1) \\ \vdots \\ \Delta u(k+N-1) \end{bmatrix}$$

$$\Phi_1 = \begin{bmatrix} CB & 0 & \dots & 0 \\ CAB + CB & CB & \dots & 0 \\ \vdots & \vdots & \ddots & 0 \\ CA^{N-1}B + CA^{N-2}B + \dots + CB & \dots & \dots & CB \end{bmatrix}$$

$$M = \begin{bmatrix} CA \\ CA^2 \\ \vdots \\ CA^N \end{bmatrix} \quad \Phi_2 = \begin{bmatrix} CB & 0 & \dots & 0 \\ CAB & CB & \dots & 0 \\ \vdots & \vdots & \ddots & 0 \\ CA^{N-1}B & CA^{N-2}B & \dots & CB \end{bmatrix} \quad (14)$$

The cost function used for the optimization contains terms related to both the output error and the input effort, where the emphasis between one and the other can be shifted by using the weighting matrix λ^2 , and is shown in Eq. (15). The output error is the difference between the predicted output $\hat{y}_p(k+j)$ and the reference $r(k+j)$ at each timestep $j = 1 \dots N$, whereas the input effort is defined by how much the control input changes between each timestep.

$$J_{MPC}(\Delta u, k) = \sum_{j=1}^N ((\hat{y}_p(k+j) - r(k+j))^T (\hat{y}_p(k+j) - r(k+j))) + \sum_{j=0}^{N_c} ((\Delta u(k+j))^T \lambda^2 (\Delta u(k+j))) \quad (15)$$

This cost function can be written in the standard Quadratic Programming (QP) form (see Appendix B-B)

$$J(\Delta u, k) = \frac{1}{2} \Delta u^T H \Delta u + F^T \Delta u \quad (16)$$

where

$$H = 2(\Phi_1^T \Phi_1 + \lambda^2) \quad (17)$$

$$F = -\mathbf{r}^T \Phi_1 + \bar{\mathbf{y}}^T \Phi_1 + \mathbf{u}(k-1)^T \Phi_2^T \Phi_1$$

Furthermore, there are two constraints on the input. Firstly, the input is limited to a range of $[\mathbf{u}_{\min}, \mathbf{u}_{\max}] = [-1, 1]$, which for the IIO model translates to

$$\begin{bmatrix} -u(k-1) + u_{\min} \\ -u(k-1) + u_{\min} \\ \vdots \\ -u(k-1) + u_{\min} \end{bmatrix} \leq \begin{bmatrix} P \\ -P \end{bmatrix} \leq \begin{bmatrix} -u(k-1) + u_{\max} \\ -u(k-1) + u_{\max} \\ \vdots \\ -u(k-1) + u_{\max} \end{bmatrix} \quad (18)$$

where

$$P = \begin{bmatrix} \Delta u(k) \\ \Delta u(k+1) + \Delta u(k) \\ \vdots \\ \Delta u(k+N-1) + \dots + \Delta u(k) \end{bmatrix} \quad (19)$$

Secondly, a control horizon constraint N_c is in place which forces the last $N - N_c$ inputs to remain constant, reducing the amount of free variables the optimization will have to take into account and thus lowering the computational power required. A value of $N_c = 10$ was chosen, corresponding to half of the prediction horizon.

The total problem can then be formulated as

$$\begin{aligned} \min_{\Delta u} \quad & J(\Delta u, k) \\ \text{s. t.} \quad & \text{Eq. (18),} \\ & \Delta u(k + N_c + j) = 0, \quad j = 0, \dots, N - N_c - 1 \end{aligned} \quad (20)$$

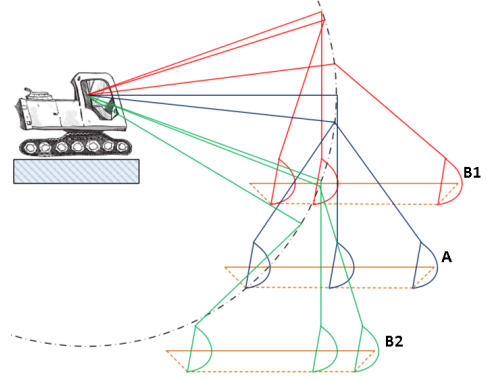
This was implemented in Matlab using a QP solver based on the KWIK algorithm [31]. For every controller interval a *cold start* is used which determines the unconstrained solution, and then checks whether this violates the constraints. If this is the case, an active set method is used to determine which constraints are relevant in the current solution space. This creates a subset of inequalities to be used during the search, which increases convergence speed.

D. Simulation task setup

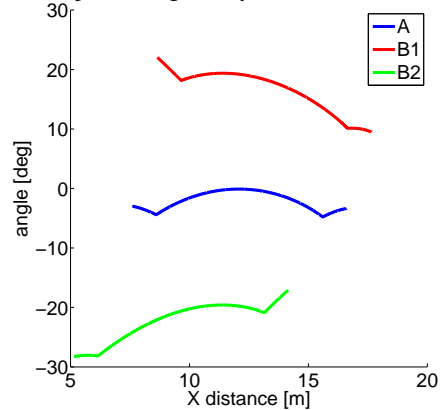
In order to evaluate the controller three tasks of various difficulty were constructed. All three tasks (A, B1, B2) consist of a 9 meter long path where the first and the last meter are reserved for entering and leaving the soil, leaving a horizontal part of 7 meters. Each task is performed at its own specific location, indicated in Fig. 9a by the same name as the name of the task.

The main difference a change in digging position makes is a change in how the boom should move in order to compensate for the circular motion of the stick. The easier task *A* is chosen such that at the center of the digging path the stick is vertical as shown in Fig. 9a, meaning that the horizontal path is split 50/50 for downwards or upwards boom compensation. As seen in Fig. 9b this means that the necessary motion of the boom is symmetrical. The more difficult tasks *B1* and *B2* are a-symmetrical and have a 75/25 and 25/75 split, respectively, increasing the complexity of the task.

Using these three tasks, three situations are evaluated in order to understand how the controller functions and what effect various tuning parameters have on the performance. These situations are:



(a) Visualization of the digging positions for the easy task (A) and difficult tasks (B1 and B2). The initial soil is always flat, and the desired paths are given by the dotted lines.



(b) Boom angle reference for the three tasks.

Fig. 9: The three digging tasks A, B1 and B2 at their respective locations. The bottom figure shows the difference in the reference for the boom angle as a result of the change in digging positions.

- Situation 1: Task A, B1 and B2 with *constant* soil.
- Situation 2: Task B1 with variable soil, in which a soft-to-hard soil transition occurs at two-thirds of the digging path. The controller is evaluated once with and once without parameter estimation.
- Situation 3: Task A with constant soil, with varying values for input weights λ^2 .

Note that for all three evaluated situations digging is performed from right to left.

E. Simulation task results

1) *Situation 1*: Fig. 10 shows that the adaptive MPC is capable of tracking the reference closely on all three locations, without requiring additional tuning. In order to quantify the tracking performance the commonly

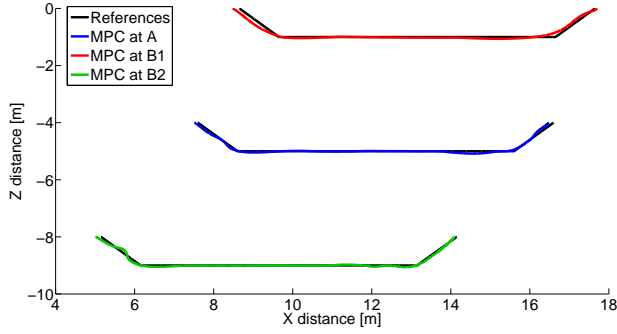


Fig. 10: Situation 1: MPC trajectories at the three locations with *constant* soil. The RMSE is 0.0242, 0.0420 and 0.0215 for tasks A, B1 and B2 respectively. Note that for all three evaluated situations digging is performed from right to left.

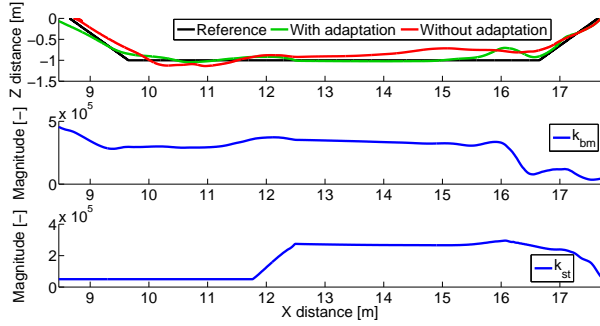
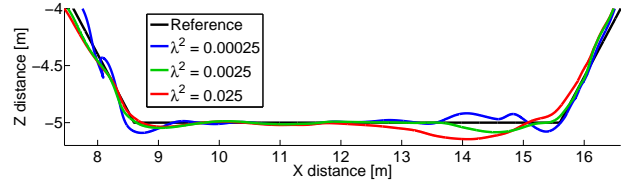


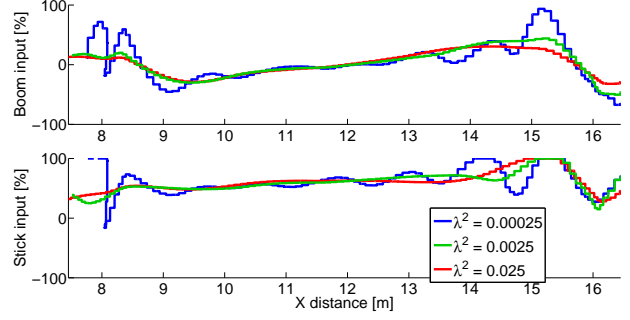
Fig. 11: Excavator performance for task B1 with and without parameter estimation. The endpoint trajectories with (green) and without (red) parameter adaptation are shown in the upmost subplot, and the input gain adaptations k_{bm} and k_{st} in the middle and bottom subplot, respectively. The difference in RMSE is notable; 0.0621 with adaptation and 0.1351 without.

used Root Mean Square Error (RMSE) between the reference and system output can be calculated for all three situations and is indicated in the caption of Fig. 10. A visual representation of the determination of the RMSE is provided in Appendix E, Fig. 24.

2) *Situation 2*: In order to assess the importance of the parameter adaptation task B1 was performed with the inclusion of a soft-hard soil transition. The initial input gains k_{bm} and k_{st} were $0.5e^5$, for both the controller with and without parameter adaptation. The excavator initially enters soft soil on the right side of Fig. 11. A clear difference in trajectory tracking can be seen here, most notably resulting from the increase in both gains k_{bm} and k_{st} during the first half the digging path. This adaptation leads to predictions that are closer to the



(a) Endpoint trajectories for task A with various input weights. RMSE is 0.0295, 0.0242, and 0.0476 for $\lambda^2 = 0.00025$, 0.0025, and 0.025 respectively.



(b) Boom and stick inputs for task A with various input weights.

Fig. 12: Situation 3: evaluation of the effect of varying input weights. The endpoint trajectories (a) resulted from the control inputs provided in (b), which were produced with $\lambda^2 = 0.00025$ (blue), 0.0025 (green), and 0.025 (red). The differences in input smoothness are quantified in Table III.

actual output, resulting in better trajectory tracking.

3) *Situation 3*: While reference tracking is usually the most important task of a controller, the importance of input effort should not be forgotten. This is especially vital for this study as the eventual goal is to provide human operator with useful guidance, which means high frequent inputs are especially undesirable. In this situation controller behavior is evaluated for three different values of the weighting term λ^2 .

Fig. 12 shows that, as expected, performance decreases when the input weights are increased, as smoother inputs are preferred. However, decreasing the weights too much results in jittery behavior. As a result, the RMSE as indicated in the caption of Fig. 12a is lowest for $\lambda^2 = 0.0025$.

In order to objectively quantify the differences in input smoothness a two-step filtering process was taken. Firstly, interpolation was applied in order to remove the effects of the discretization. Subsequently, a normalized anti causal second order high-pass Butterworth filter with a cutoff frequency of 0.5 Hz was applied. Fig. 22 in Appendix E shows an example of this approach. Essentially, this approach de-trends the input signal while retaining

TABLE III: Situation 3: Absolute Mean (AM) and Standard Deviation (SD) of filtered input signals for various λ^2 . (Units: percentage points, abbreviated as %_p)

	Input 1		Input 2	
	AM [% _p]	SD [% _p]	AM [% _p]	SD [% _p]
$\lambda^2 = 0.00025$	4.30	6.23	4.35	7.02
$\lambda^2 = 0.0025$	0.65	1.07	0.83	1.74
$\lambda^2 = 0.025$	0.29	0.47	0.43	0.89

the frequencies of interest. From this remainder of the data the Standard Deviation (SD) and absolute mean (AM) were determined as an indicator of the smoothness of the input signals and are shown in Table III. The results show that an increase in λ^2 results in a lower SD and AM, indicating smoother input signals.

F. Discussion on the Model Predictive Controller

The simplified model defined in Section III-A was used for two parts of the control algorithm. Firstly, a linearized version was used as the internal model on which the MPC based its algorithms. Secondly, the nonlinear variant was used by Extended Kalman Filter in order enable online adaptation. The combination of these two techniques results in smooth inputs and a low tracking error while still being computationally simple, allowing real-time implementation. Furthermore, this combination also makes the simplified model rather robust. A relatively low-level simplified model can still result in good performance, since the EKF aims to steer it towards the behavior of the true system and can thus reduce the influence of modelling errors.

The combination of the internal model and EKF was validated using several test cases. Situation 1 tested the MPC's capability of controlling the system at several different locations. This shows that the internal model which is linearized at every controller interval can approximately describe the behavior of the excavator over the whole workspace. Situation 2 showed the necessity of the online parameter adaptation, demonstrating a two-fold decrease in tracking error. Situation 3 focused on the trade-off between performance and input effort present in the MPC algorithm. An interesting effect is seen here; there exists a point after which focusing less on input effort does not result in an increase in performance. This is most likely due to inaccuracies in the internal model. Essentially, placing a large importance on performance will result in aggressive inputs, relying almost solely on the feed-forward predictions of the internal model. Inaccuracies can thus result in overshooting and jittery behavior. This is in its turn detrimental for the EKF, as the dead-band phenomenon in the valves and the

disparity between upward and downwards motions can result in fluctuations in the parameter estimation.

This portrays some of the downsides of the implementation of the online adaptation for the MPC algorithm used here. At every controller interval the current linear model, using the current estimated parameters, is used in order to determine its future input sequence. During the execution of this algorithm the linear model stays constant as future fluctuations of the parameters are unknown, even though in reality the estimated parameters these vary. Furthermore, the parameter adaptation is not instantaneous and as a result large, frequent input variations deteriorate controller performance.

These issues could be resolved in future work by implementing a learning algorithm, which could memorize previous digging iterations and could provide a more suitable model when frequent switching behavior is present. This could provide the MPC with a reasonable guess about future values of these estimated parameters.

G. Sub-conclusions on the Model Predictive Controller

From the results of the simulation tasks it can be concluded that the MPC in combination with the Extended Kalman Filter is able to control the complex excavator model at various locations and for a priori unknown, varying soil profiles. The results shown here indicate that the MPC is capable of achieving low tracking errors for various tasks while providing smooth inputs. Furthermore as described in Section I, MPC is based on similar underlying principles as human control.

These results, combined with the similarities on which the control principles of both the MPC and the human operator are based on show promising prospects for the application of continuous guidance.

IV. HUMAN FACTORS EXPERIMENT

The goal of this excavator simulator experiment is twofold. Firstly, the *similarity* between the control inputs of the operators and the designed MPC are compared for a well-trained situation (task A) in which the task was relatively simple and operators received extensive training. This was assumed to enable operators to construct a reasonably accurate internal model, and thus produce accurate control inputs. Secondly, *performance* is compared in terms of smoothness of the control inputs and trajectory tracking error for tasks of varying difficulty (tasks A, B1, and B2). Furthermore, the reaction to a task where an unseen boulder was located on the trajectory that would require an unintended deviation from the target trajectory was compared.

A. Method

1) *Participants*: 8 participants (1 female), all right-handed, between 23-57 years old (Mean = 28.5, SD = 10.7) volunteered for the excavation simulator experiment.

2) *Apparatus*: The experiment was conducted using a type MPC270 Bachmann real-time computer, ensuring a consistent match between simulation time and real time. The complex excavator model described in Section II was uploaded onto the Bachmann and connected to the commercially available *DipMate 2* visualization software, version 3.20, developed by the company *SeaTools*. An example of the visualization including a reference and one completed trial is shown in Fig. 13. This visualization was shown on a Dell P2210 22 inch monitor with a refreshing rate of 60 Hz, while the underlying simulation and data logging ran with a sampling frequency of 500 Hz. The subjects were tasked with controlling the excavator using a 2 Degree of Freedom (DoF) *Thrustmaster T.16000M* joystick.

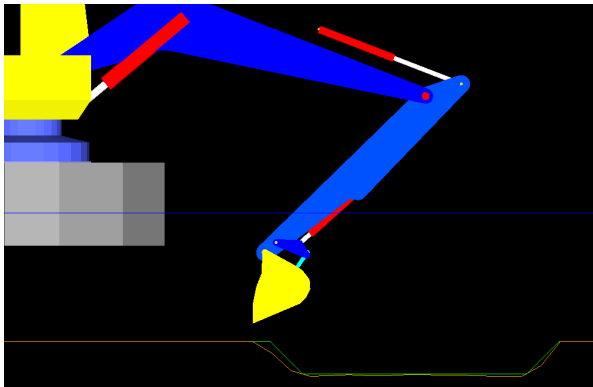


Fig. 13: DipMate simulation software including the desired trajectory (green), water level (blue) and soil profile after a trial (brown).

3) *Experimental design*: The total experiment consisted of four stages which are shown in Fig. 14. Firstly, the operator could get accustomed to the system in the familiarization stage. Secondly, the operator entered the *easy* stage in which the digging task was relatively simple due to the constant soil and the symmetric reference (shown in Fig. 9) simplifying the calculation of the inverse kinematics, which subjects subconsciously perform. Thirdly, the *difficult* stage was performed in which the digging location and soil conditions varied. Lastly, the final stage consisted of a single trial in which an unseen boulder was inserted on the digging path, requiring an unintended deviation from the target trajectory.

Experiment setup

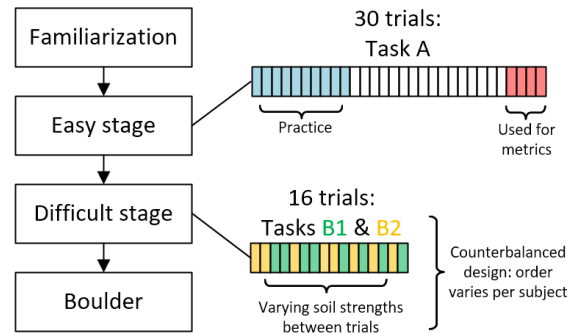


Fig. 14: Setup of the experiment. All subjects follow the same process, except for the difficult stage in which the order of the tasks and types of soil varied per subject. The 5 soil types used are indicated in Fig. 15.

During the *easy* and *difficult* stage a timer was shown on the screen and subjects were tasked with completing the digging trajectory between 20-25 seconds. Deviations above or below this time led to the experimenter orally motivating subjects to increase or decrease their digging speed. Prior to the experiment an informed consent form was signed, which explained the purpose, procedures and provided various task instructions (Appendix I). This instructed the subjects on how to use the joystick, explained the order and length of the tasks. Furthermore, it explained the subjects were expected to follow the trajectory while staying within a time of 20-25 seconds while avoiding backwards motions to correct for previous deviations from the trajectory. Subjects were allowed to take breaks or terminate the experiment at any time without negative consequences.

a) *Familiarization stage*: The familiarization was structured in a set of 7 simple tasks, individually explained in Appendix C, performed subsequently. These tasks aided the subject in developing a better understanding of the system. This was especially necessary since excavators are systems with which the general population does not have any experience with. These tasks allowed the subject to experience several characteristics of the system. Firstly, the subjects were able to relate the direction of the movements of the excavator to the direction in which they moved the joystick. Secondly, subjects understood end-point (cartesian) control was not used, and they would have to account for the circular motions of both the boom and the stick while digging straight lines. Thirdly, the effect low or high frequent inputs had on the output of the excavator was experienced.

Finally, the subjects were able to get accustomed to the visualization software.

b) Easy stage: task A: Performance and control effort are considered to be the main driving factors of motor learning [32], but it was shown that subjects initially mostly optimize for performance, and that adaptation based on control effort is driven at a much slower rate [33]. Furthermore, the idea behind satisficing control [18] states that human operators attempt to obtain a satisfactory performance level, but do not minimize performance further if it requires too many resources (control effort, mental workload). Based on this knowledge, task A (see Fig. 9) was performed 30 times in the *easy* stage. By performing this large amount of trials it was expected that after the initial increase in performance deemed satisfactory by the operator, the subjects would then attempt to decrease their control effort while maintaining a satisfactory level of performance.

In this task the location of the digging trajectory and the strength of the soil was kept constant throughout all 30 trials. Furthermore, the subjects were explained that the first 10 trials were training trials, and that their performance during these trials was not taken into account. These trials provided the opportunity for exploration in which subjects were able to wildly vary their control strategies without negative consequences, enabling them to get a better feeling for the system and thus reducing the probability of them purely relying on feedback. Finally, the last four trials are used for the calculation of metrics, as it is assumed that the best performance and control effort are achieved in the trials in which the subjects have had the most experience with the system.

c) Difficult stage: tasks B1 and B2: The next stage of the experiment attempted to evaluate performance and control effort for a new, more difficult task and consisted of 16 trials which were evenly split up between tasks B1 and B2. These tasks are indicated with red (B1) and green (B2) lines in Fig. 9. As seen in Fig. 9b these two tasks require a-symmetrical movement of the boom. Furthermore, variations in soil strength were applied. The controller was compared to the humans on both locations B1 and B2. However, while it is necessary to obtain multiple repetitions of the desired condition in order to reduce inherent human variability for the comparison, too many repetitions would cause the subjects to memorize the transition location and changes in strength within the task. In order to avoid this, multiple types of soil patterns were constructed as shown in Fig. 15. Only one type was evaluated as the 'desired' soil type for either task B1 or B2 (type 2 for task B1, type 3 for task B2), and the other soil types were implemented

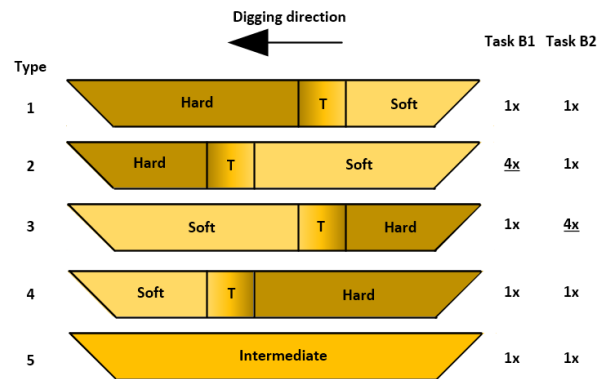


Fig. 15: The arrangement of 5 different soil types in the difficult stage, for task B1 and B2. Both task B1 and B2 consist of 8 trials, in which the frequency with which each soil type was used for the respective task are indicated by the rightmost numbers. Metrics of tasks B1 and B2 are evaluated for soil types 2 and 3, respectively, where the 4 trials with soil types 1, 4 and 5 are only used to introduce randomness to avoid memorization.

solely to create randomness and were not evaluated. In total, each task thus consisted of 8 trials, of which 4 trials contained the 'desired' type and of which the other 4 trials were one repetition of each of the other 4 soil types. Finally, the order of these 16 trials was determined using a counterbalanced latin square design.

d) Boulder stage: The final stage of the experiment featured only 1 trial, performed on location A. An impenetrable boulder was located halfway during the digging path about which the subjects were uninformed. Passing the 1 meter tall boulder required a deviation of at least half a meter from the target trajectory to pass under or over the boulder. No explanation was provided to the subject, except the conformation that this was not a simulation error, and that subjects were still expected to complete the task.

4) Dependent measures: The metrics used can be grouped according to their use for the two goals of the experiment.

a) Similarity in task A: The similarity between the MPC and the subjects is evaluated for the well-trained task (A) only, in which operators are assumed to have trained a decently accurate internal model, and can hence provide accurate control inputs.

- The *Variance Accounted For (VAF) [%]* is used to determine the degree of similarity between two signals, ranging between 0% – 100%. The VAF between the two signals u and u_{MPC} and can be constructed as:

$$VAF = \max\left(1 - \frac{\text{var}(u - u_{MPC})}{\text{var}(u)} * 100\%, 0\right) \quad (21)$$

b) *Performance*: The performance is measured using two metrics, both of which have been used previously for the simulation study.

- The *Root Mean Square Error (RMSE) [m]* indicates the difference between the reference trajectory and the performed trajectory. An example of its determination can be seen in Appendix E, Fig. 24.
- The *Standard Deviation of the control input (SD) [percentage points, abbreviated as %_p]* represents the smoothness of the input signals. This metric was calculated by first interpolating the input signals in order to remove the effects of the discretization. Subsequently, a normalized anti causal high-pass second order Butterworth filter with a cutoff frequency of 0.5 Hz was applied, remaining only with the high frequent components of the input signals. From this remainder the standard deviation was taken. Fig. 22 in Appendix E shows an example of this approach.

B. Results

1) *Similarity in task A*: Fig. 16 depicts the 4 final trials of the best performing subject for task A, alongside the performance of the MPC. Fig. 17a shows the desired trajectory and the tracking performance of both the subject and the MPC. The inputs provided to both the boom and the stick the operator used to realise these trajectories are shown in Fig. 16b and Fig. 16c. Note that for clarity reasons the discretization effects of all input signals are removed with a normalized anti causal low-pass second order Butterworth filter with a cutoff frequency of 5 Hz. Clearly, the MPC shows smaller deviations from the target trajectory. The boom inputs lead to two observations. Firstly, the MPC provides a much smoother boom input than the subject. Secondly, a clear similarity is present between the boom input of the controller and the operator. This similarity is not present in the stick inputs, which is not unexpected due to the nature of the horizontal trajectory tracking task, in which the position of the boom determines the tracking error while the stick only controls the digging velocity.

The amount of variability still present in the provided inputs indicates that the subject is not yet trained to the level of an expert. This is indeed reflected in the performance of all other subjects during task A. Learning curves plotted for both task accuracy and input smoothness over all trials of the task show a very weak

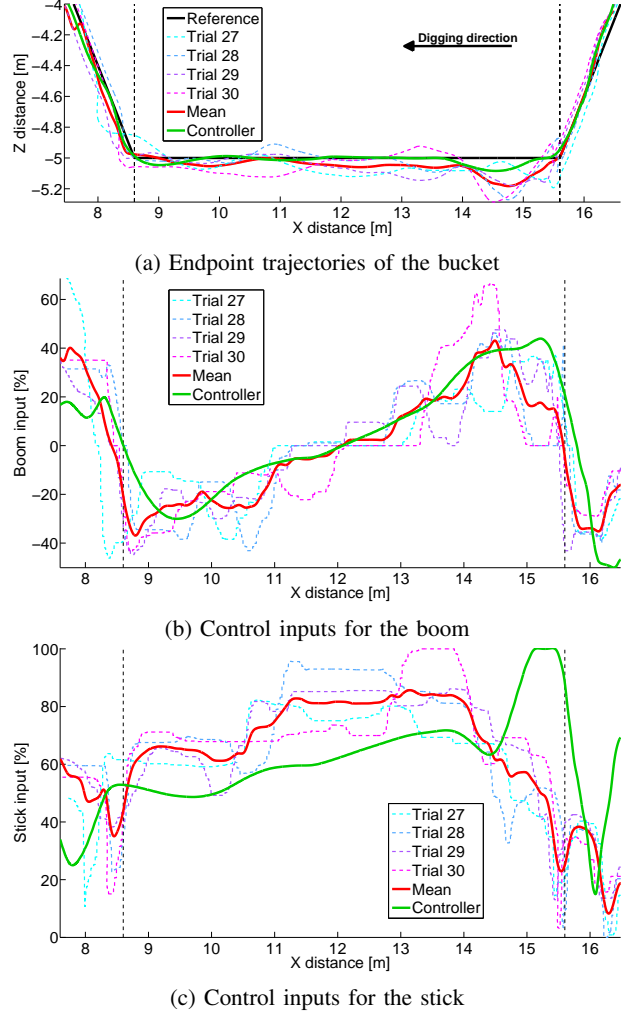
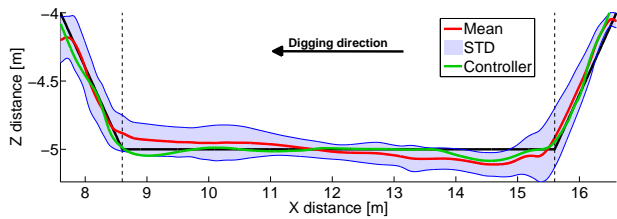
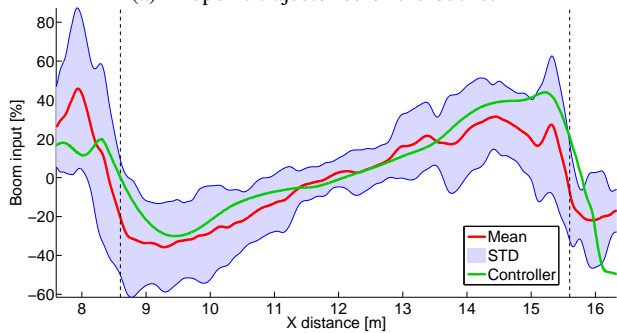


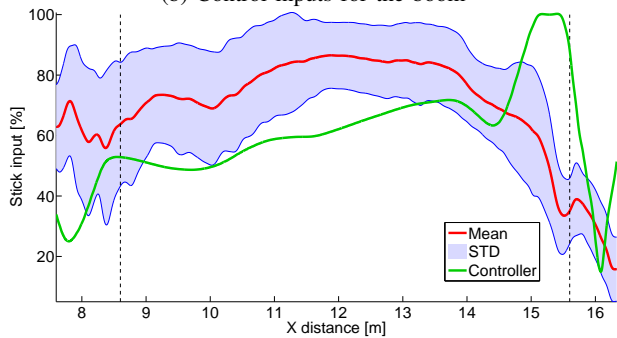
Fig. 16: Trajectories and control inputs of the last 4 trials of subject 7 (the best performing subject in terms of trajectory tracking errors) in task A. The three panels show the endpoint trajectories of the bucket (a) and the control inputs for the boom (b) and stick (c). The mean (red) over the last four trials (dashed lines) are shown against the controller (green). The vertical, dashed black line indicates the start and end of the horizontal part of the trajectory. Significant variability is still present, however it is noticeable that the boom inputs of the MPC and operator are quite comparable.



(a) Endpoint trajectories of the bucket



(b) Control inputs for the boom



(c) Control inputs for the stick

Fig. 17: Similarly to Fig. 16, the three panels show the endpoint trajectories of the bucket (a) and the control inputs for the boom (b) and stick (c) for task A. The mean of the last four trials of all subjects (red) and its standard deviation (blue area) are compared against the controller. The vertical, dashed black line indicates the start and end of the horizontal part of the trajectory.

learning effect (Appendix D), indicating that even the easier task was of considerable difficulty for the subjects. This means an "expert" operator with which to compare the controller is not present.

In order to attenuate the influence of human variability and analyse whether the MPC and subjects do indeed exhibit similar behavior even though a true expert is not present, the inputs of the last 4 trials of each subject are averaged and undesired high frequent noise is smoothened using a 5 Hz low-pass filter. This is done for individual subjects (as depicted for one subject with the

TABLE IV: Control behavior similarity. The Variance Accounted For (VAF) values between the controller and the mean of the last 4 trials per subject and the total group, for task A, are shown. The boom inputs show a high quality fit while the stick inputs show a mismatch.

	VAF [%]	
	Boom input	Stick input
Subject 1	71.0	0
Subject 2	80.4	0
Subject 3	46.3	0
Subject 4	66.8	0
Subject 5	69.6	0
Subject 6	0	0
Subject 7	75.4	0
Subject 8	76.3	0
Total group	73.1	0

red line in Fig. 16) and for the total group. The means of the total group are plotted alongside their standard deviation in Fig. 17. In order to more objectively determine the similarity between the controller and the operator, the VAF is used and reported in Table IV, showing both the VAF scores per individual subject and for the total group. While the stick inputs show a mismatch, a high quality fit is found for the boom inputs for both individual subjects and the group as a whole except for Subject 6, who exerted a large amount of bang-bang control (clarification: Appendix G, Fig. 30).

2) *Performance*: The performance metrics for all three tasks are shown in Fig. 18. The adaptive MPC shows better performance on all three tasks than human operators. In terms of trajectory tracking, the controller shows an RMSE that is 3.7, 3.4 and 2.2 times lower than human operators for tasks A, B1 and B2 respectively. In terms of control effort, the boom input especially shows a large difference, while the differences for the stick input are much more subtle. Human operators exhibit 5.5, 5.6 and 3.9 times as many input above a frequencies of 0.5 Hz for the boom and 2.1, 1.5 and 1.9 times as many for the stick, for task A, B1 and B2 respectively. Finally, the boulder task portrayed in Fig. 19 showed that without any prior knowledge about the existence of a boulder subjects were able to navigate past the obstacle, finish the digging task and extract the bucket from the soil (completion time in seconds: Mean = 23.9, SD = 4.6). On the other hand, the controller got stuck on the boulder and did not attempt to deviate from its pre-set trajectory.

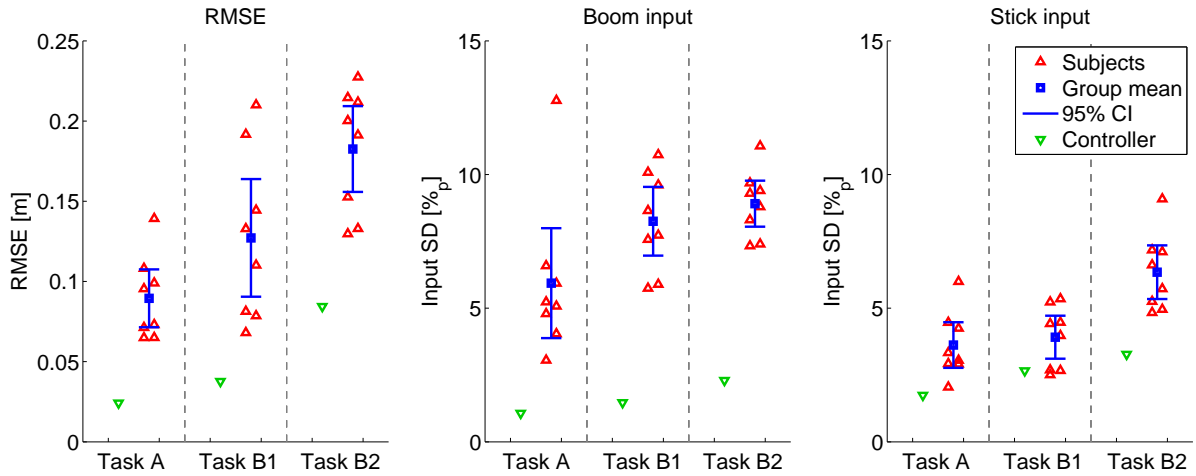


Fig. 18: RMSE and SD of both inputs for all tasks. Each individual red triangle represents the mean value of the respective metric for the last 4 trials for one subject, for the respective task. The 95% Confidence Interval (CI) is indicated with the blue lines. The MPC shows better trajectory tracking and smoother inputs for every task. The Mean (M) and SD of the completion times of the average subject in seconds were: Mean = 19.4, SD = 1.74 (A), Mean = 21.8, SD = 2.95 (B1), Mean = 17.8, SD = 1.80 (B2), whereas the controller had completion times of 19.5 (A), 19.9 (B1) and 18.1 (B2).

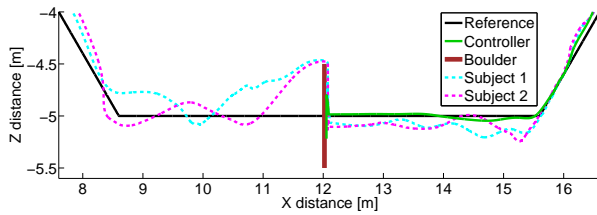


Fig. 19: Boulder encounter for two typical subjects and the controller. While the MPC gets stuck on the boulder, human operators manage to surpass the obstacle.

C. Discussion on the human factors experiment

The aim of this human factors experiment was twofold. It attempted to evaluate whether the MPC controls the offshore excavator in a similar manner as human operators, and whether it is capable of performing better than the human.

1) *Similarity*: The results show a clear similarity between the inputs provided to the boom. The VAF for most individuals and the group is above 70%, indicating a high quality fit. Subject 6 however shows a VAF of 0%, which is due to the extreme use of bang-bang control for this subject. The SD of the boom input for task A of this subject indeed lies 2.3 standard deviations above the group average, indicating that extremely wild inputs were provided.

The results also show a clear mismatch exists between the inputs provided to the stick. This, however, is not

completely unexpected. The experimental task consisted of a mostly horizontal path, which the subjects were instructed to follow. The boom essentially provided the lateral steering whereas the stick controlled the longitudinal direction. This kind of task is therefore comparable to car-driving, where the stick is thought of as the gas pedal and where the boom is thought of as the steering wheel. Various studies focus on the application of continuous guidance to car-driving [34] [35] and the problem of conflict reduction between controller and human [14] [36]. However, all these studies demarcate the problem by imposing a fixed driving speed, and only consider the lateral aspect. This has considerable advantages which are also apparent in this thesis: it de-couples the challenging control problem, allows for easier comparison of the dependent variables of interest, and reduces the variability between operators. The latter is perhaps the most challenging issue with the longitudinal component: individual operators may have different preferences which may still all result in equally good trajectories, as long as the lateral steering is performed adequately. As of recently research towards developing individual models for various types of operators [37] [38], however much more research in this field is necessary before guidance can be provided on both degrees of freedom.

2) *Performance*: The controller shows a more than threefold reduction in trajectory tracking error for tasks A and B1 and a twofold reduction for task B2. Moreover,

it does so while providing smoother inputs and thus lower control effort; human operators exhibit 4 to 5 times as many inputs above a frequencies of 0.5 Hz for the boom and 1.5 to 2 times as many for the stick. Furthermore, it is seen that unforeseen variations in soil strength affect both controller and operator, especially in Task B2 which shows a large decrease in performance for both controller and all subjects. This is most likely due to a very difficult to deal with transition from hard soil to very soft soil, leading to overshoot and wild, corrective inputs.

Finally, the boulder task shows one of the major advantages of keeping the human in the loop. While the MPC does perform better than the human, it is only capable of controlling the system in situations for which it has explicitly been programmed. When an obstacle is introduced that neither the MPC nor the human operators have had any experience with, human operators are capable of adapting on the fly whereas the controller is not able to proceed. Until a point is reached in which automation is so advanced and can truly control a system for every possibly situation, human operators will be needed. As argued in Section I, regardless of whether the human and automation interact through continuous guidance (shared control) or supervisory control, a more human-centered approach is beneficial. Herein lies the strength of human-like control as applied in this thesis: by providing control that matches the operator's intents, the operator is hypothesized to understand the automation better, which could reduce the amount of conflicts in a continuous guidance setting and reduce issues such as a loss of situational awareness.

D. Sub-conclusions on the human factors experiment

The human factors experiment show that the Adaptive MPC is capable of achieving up to 2-3 times more accurate reference tracking while providing smoother inputs, containing around 4-5 times (boom) and 1.5-2 times (stick) fewer inputs above a frequency of 0.5 Hz than the subjects, on all three evaluated tasks. Additionally, a high quality fit ($VAF > 70\%$) is found between the boom inputs of the subjects and the controller, while a mismatch exists between the stick inputs. The combination of achieving better performance while providing human-like boom inputs makes for a compelling argument towards applying the MPC for continuous guidance, however currently guidance should only be applied on the boom. Lastly, the necessity of keeping the human in the loop is shown by a trial with an unmovable disturbance. While the controller was not able to proceed, all subjects were able to adapt to this unforeseen disturbance and complete the task.

V. CONCLUSIONS AND FUTURE WORK

1) In this work a human-centered approach to excavator control is taken by focusing on the design and evaluation of a human-like controller to partially automate excavator operations.

a) A complex excavator model was constructed by extending a generic excavator model (based on literature) with a hydraulic system and a soil model, and exhibits relevant and realistic (nonlinear) behavior in simulations, showing itself to be a more accurate reflection of a real excavator than the approximate models currently used in literature.

b) In order to provide human-like control, an adaptive Model Predictive Controller was designed by combining standard MPC and its internal model with an Extended Kalman Filter in order to capture unmodelled and unforeseen behavior. The controller was evaluated in a simulation environment, showing low reference tracking errors and smooth inputs for various tasks, even when unknown soil variations were applied.

c) A comparison between the controller and human operators was made in a human factors experiment, which showed a high quality fit ($VAF > 70\%$) between the boom inputs of the controller and subjects for a well-trained task, indicating human-like control. Furthermore, the adaptive MPC showed 2 to 3 times lower tracking errors and 1.5 to 5 times smoother inputs on all experimental tasks than the average subject. These results show promising application aspects for the use of Model Predictive Control for continuous guidance or more human-like supervisory control.

2) Future work should consider enhancing the MPC by allowing it to learn from previous digging iterations, such that it is capable of predicting changes of dynamics instead of solely relying on current information.

Moreover, while the boom inputs for both the subjects and the controller are similar, the stick inputs show a mismatch. This indicates that in future work guidance should either only be considered for the boom input or that additional research should be performed in order to capture a human-like velocity profile, suitable for each individual operator.

Lastly, a full-scale experiment in which continuous guidance is applied through the use of for instance Haptic Shared Control should be performed to examine whether the guidance is indeed received as desirable, now that this preliminary human factors experiment has shown promising application aspects for the use of MPC in human-like control.

REFERENCES

- [1] P D Lawrence, S E Salcudean, N Sepehri, D Chan, S Bachmann, N Parker, M Zhu, and R Frenette. Coordinated and Force-Feedback Control of Hydraulic Excavators. *Electrical Engineering*, 1995.
- [2] A.J. Kempkes. Dredging Monitoring System for marine excavators.
- [3] Thomas B Sheridan. *TeleRobotics*. 25(4), 1989.
- [4] P. M Fitts. Human engineering for an effective air-navigation and traffic-control system. 1951.
- [5] Thomas B Sheridan. *Human and Computer Control of Undersea Teleoperators*. 1978.
- [6] C.E Billings. *Aviation Automation: the search for a Human-Centered Approach*, 1997.
- [7] Lianne Bainbridge. Ironies of automation. *Automatica*, 19(6):775–779, 1983.
- [8] Mica R Endsley. *Automation and Situation Awareness. Automation and Human Performance: Theory and Applications*, pages 163–181, 1996.
- [9] M R Endsley and D B Kaber. *Level of automation effects on performance, situation awareness and workload in a dynamic control task.*, volume 42. 1999.
- [10] By Peter A Hancock, Richard J Jagacinski, Raja Parasuraman, Christopher D Wickens, Glenn F Wilson, and David B Kaber. *Human-Automation Interaction Research: Past, Present, and Future*. (April):9–14, 2013.
- [11] David A. Abbink, Mark Mulder, and Erwin R. Boer. Haptic shared control: Smoothly shifting control authority? *Cognition, Technology and Work*, 14(1):19–28, 2012.
- [12] Mark Mulder, David A. Abbink, and Erwin R. Boer. Sharing Control With Haptics: Seamless Driver Support From Manual to Automatic Control. *Human Factors: The Journal of the Human Factors and Ergonomics Society*, 54(5):786–798, 2012.
- [13] Franck O. Flemisch, Johann Kelsch, Christian Loper, Anna Schieben, Julian Schindler, and Heesen Matthias. Cooperative Control and Active Interfaces for Vehicle Assistance and Automation. *FISITA World Automotive Congress*, (2):301–310, 2008.
- [14] Rolf Boink, Marinus M. Van Paassen, Mark Mulder, and David A. Abbink. Understanding and reducing conflicts between driver and haptic shared control. *Conference Proceedings - IEEE International Conference on Systems, Man and Cybernetics*, 2014-Janua(January):1510–1515, 2014.
- [15] Daniel M. Wolpert, R. Chris Miall, and Mitsuo Kawato. Internal models in the cerebellum. *Trends in Cognitive Sciences*, 2(9):338–347, 1998.
- [16] Mitsuo Kawato. Internal models for motor control and trajectory planning. *Current Opinion in Neurobiology*, 9(6):718–727, 1999.
- [17] M. D. Mesarovic and Y. Takahara. On a qualitative theory of satisfactory control. *Information Sciences*, 4(3-4):291–313, 1972.
- [18] J M Hoc. Cognitive Control Dynamics for Reaching a Satisficing Performance in Complex Dynamic Situations. 1(1):22–55, 2007.
- [19] D a Abbink and M Mulder. Exploring the Dimensions of Haptic Feedback Support in Manual Control. *Journal of Computing and Information Science in Engineering*, 9(March 2009):011006, 2009.
- [20] James B. Rawlings. Tutorial overview of model predictive control. *IEEE Control Systems Magazine*, 20(3):38–52, 2000.
- [21] Gregory L. Plett. Extended Kalman filtering for battery management systems of LiPB-based HEV battery packs - Part 3. State and parameter estimation. *Journal of Power Sources*, 134(2):277–292, 2004.
- [22] Yang Liu, Mohammad Shahidul Hasan, and Hong Nian Yu. Modelling and Remote Control of an Excavator. *International Journal of Automation and Computing*, 7(3):349–358, 2010.
- [23] Antti J. Koivo, M. Thoma, E. Kocaoglan, and J. Andrade-Cetto. Modeling and Control of Excavator Dynamics during Digging Operation. *Journal of Aerospace Engineering*, 9(1):10–18, 1996.
- [24] Pyung Hun Chang and Soo-jin Lee. A straight-line motion tracking control of hydraulic excavator system. 12:119–138, 2002.
- [25] F A Bender, M Sonntag, and O Sawodny. Nonlinear model predictive control of a hydraulic excavator using Hammerstein models. *Journal of Process Control* 7, 31-41, pages 31–41, 2015.
- [26] M. H. Chiang and C. C. Huang. Experimental implementation of complex path tracking control for large robotic hydraulic excavators. *International Journal of Advanced Manufacturing Technology*, 23(1-2):126–132, 2004.
- [27] A J Koivo. Kinematics of excavators (backhoes) for transferring surface material. 7(1):17–32, 1994.
- [28] Shahram Tafazoli, Peter D. Lawrence, and S. E. Salcudean. Identification of inertial and friction parameters for excavator arms. *IEEE Transactions on Robotics and Automation*, 15(5):966–971, 1999.
- [29] Sape A Miedema and Djurre Zijsling. Hyperbaric Rock Cutting. *Proceedings of the ASME 31th International Conference on Ocean, Offshore and Arctic Engineering*, (March):1–14, 2012.
- [30] Eric a Wan and Alex T Nelson. *Dual extended kalman filter methods*, volume 5. 2001.
- [31] L. T. Biegler and Schmid C. Quadratic Programming Methods for Reduced Hessian SQP. *Computers & Chemical Engineering*, 18(9):817–832, 1994.
- [32] Jeremy L Emken, Raul Benitez, Athanasios Sideris, James E Bobrow, and David J Reinkensmeyer. Motor Adaptation as a Greedy Optimization of Error and Effort. pages 3997–4006, 2007.
- [33] Edwin H F Van Asseldonk, Martijn Wessels, Arno H A Stienen, Frans C T Van Der Helm, and Herman Van Der Kooij. Journal of Physiology - Paris Influence of haptic guidance in learning a novel visuomotor task. *Journal of Physiology - Paris*, 103(3-5):276–285, 2009.
- [34] David A. Abbink, Diane Cleij, Mark Mulder, and Marinus M. Van Paassen. The importance of including knowledge of neuromuscular behaviour in haptic shared control. *Conference Proceedings - IEEE International Conference on Systems, Man and Cybernetics*, pages 3350–3355, 2012.
- [35] J Navarro F Mars M S Young. Lateral control assistance in car driving : classification , review and future prospects. (July 2010), 2011.
- [36] Franck Mars, Mathieu Deroo, and Jean-michel Hoc. Analysis of Human-Machine Cooperation When Driving with Different Degrees of Haptic Shared Control. 7(3):324–333, 2014.
- [37] Wilko Schwarting, Javier Alonso-mora, Liam Paull, Sertac Karaman, and Daniela Rus. Parallel Autonomy in Automated Vehicles : Safe Motion Generation with Minimal Intervention. 2017.
- [38] Virgilio Gruppelaar. Measuring and modeling the role of time thresholds in drivers’ pedal control inputs during cornering speed adaptation. pages 1–18.
- [39] Vincent Honing, Tricia L Gibo, Roel J Kuiper, and David A Abbink. Training with haptic shared control to learn a slow dynamic system. 2014.

APPENDIX A
ADDITIONAL MODELLING EXPLANATIONS

A. Hydraulic equations

By assuming incompressible, laminar flow with negligible losses, the volumetric flow through the valve can be calculated using Bernoulli's equation

$$p_1 + \frac{1}{2}\rho V_1^2 = p_2 + \frac{1}{2}\rho V_2^2 \quad (22)$$

in addition to the continuity equation

$$q_v = A_1 V_1 = A_2 V_2 \quad (23)$$

where q_v is the theoretical volumetric flow rate. Rewriting gives

$$q_v = A_2 \sqrt{\frac{2(p_1 - p_2)/\rho}{1 - (A_2/A_1)^2}} \quad (24)$$

By furthermore introducing the discharge coefficient C_d , $p_1 - p_2 = \Delta p$, the volumetric flow rate through the valve can be calculated as

$$Q = C_d A_2 \sqrt{\frac{2\Delta p}{\rho}} \quad (25)$$

B. Soil memory block

In order for subsequent digs to properly apply forces, the position of the soil and thus the position where the bucket comes into contact with the spring/damper systems need to be updated accordingly. This is done in the soil memory block. In this block the soil profile is stored and updated online to reflect the soil as the excavator is digging through it.

As usually done in practice, it is assumed that before digging a scan is performed, such that the current profile and depth of the seafloor is known. The horizontal axis of the seabed is then divided into blocks of 30 centimeters to lower the computational power required. Each of these block is assigned a number i , ranging from 1 (far left of the workspace) to 67 (far right of the workspace) for a workspace ranging from [0, 20] meters, where the excavator is positioned at (0,0) and the maximum extension of the excavator is always below 20 meters. Before the first dig, the a priori information is incorporated by assigning the initial depth to its respective block. During digging, the x position of the tip of the excavator's bucket indicates which block is active. If the excavator starts digging, its current depth will exceed the memorized depth and the new depth will be stored for the respective block. In this manner multiple scoops can be made while the position of the ground is continuously updated.

C. Water drag forces

Finally, drag forces as a result of moving through water are calculated by first determining which parts of the excavator are submerged and applying the standard drag force equation $F = \frac{1}{2}C_d\rho AV^2$ where the boom and stick are assumed to have a rectangular surface area, while the bucket is modelled as a hollow hemisphere. This gives drag coefficients C_d of 1.05 and 1.42, respectively.

APPENDIX B
MPC PROBLEM SETUP ELABORATION

In this appendix the implementation of the MPC algorithm is elaborated upon.

A. Prediction matrices

In it's standard form a system's state space description is:

$$\begin{aligned} x(k+1) &= Ax(k) + Bu(k) \\ y(k) &= Cx(k) \end{aligned} \quad (26)$$

Substituting to obtain the output prediction at k+1

$$y(k+1) = Cx(k+1) = C(Ax(k) + Bu(k)) \quad (27)$$

Using this approach, we can calculate multiple steps ahead based on these system matrices, the current state and future input signals as:

$$\begin{aligned} x(k+2) &= Ax(k+1) + Bu(k+1) \\ y(k+2) &= Cx(k+2) = CAx(k+1) + CBu(k+1) = CA^2x(k) + CABu(k) + CBu(k+1) \end{aligned} \quad (28)$$

Which can be repeated for an N amount of predictions and written into matrix format:

$$\begin{bmatrix} y(k+1) \\ y(k+2) \\ y(k+3) \\ \vdots \\ y(k+N-1) \\ y(k+N) \end{bmatrix} = \begin{bmatrix} CA \\ CA^2 \\ CA^3 \\ \vdots \\ CA^{N-1} \\ CA^N \end{bmatrix} x(k) + \begin{bmatrix} CB & 0 & 0 & \cdots & 0 & 0 \\ CAB & CB & 0 & \cdots & 0 & 0 \\ CA^2B & CAB & CB & \cdots & 0 & 0 \\ \vdots & \vdots & \vdots & \ddots & 0 & 0 \\ CA^{N-2}B & CA^{N-3}B & CA^{N-4}B & \cdots & CB & 0 \\ CA^{N-1}B & CA^{N-2}B & CA^{N-3}B & \cdots & CAB & CB \end{bmatrix} \begin{bmatrix} u(k) \\ u(k+1) \\ u(k+2) \\ \vdots \\ u(k+N-2) \\ u(k+N-1) \end{bmatrix} \quad (29)$$

However, the application of linearization changes this model from a model describing the entire workspace to a model that is only valid locally, around the linearization point. To compensate, the output \bar{y} and state \bar{x} at the trimmed position must be subtracted from y and x . Normally, the same would be done for the input signal, but due to the use of rate control this does not apply to the excavator. Furthermore, the rate with which the input changes is of interest, as opposed to the magnitude. In order to allow optimization of Δu instead of u the system must be translated to an Incremental Input Output (IIO) system which uses the input increment Δu .

First, the application of linearization translates the one-step ahead prediction of the standard state space to:

$$y(k+1) = \bar{y} + CA(x(k) - \bar{x}) + CBu(k) \quad (30)$$

which, when rewritten to IIO form is:

$$y(k+1) = \bar{y} + CA(x(k) - \bar{x}) + CB\Delta u(k) + CBu(k-1) \quad (31)$$

and similarly:

$$y(k+2) = \bar{y} + CA^2(x(k) - \bar{x}) + (CAB + CB)\Delta u(k) + CB\Delta u(k+1) + CABu(k-1) \quad (32)$$

Note how due to the usage of the input increment past values of Δu appear multiple times. For example: $\Delta u(k)$ affects $y(k+3)$ with a gain of $(CA^2B + CAB + CB)$. By repeating this for an N amount of predictions, and writing into a matrix format, we obtain the equations as in Eq. (13).

B. Translating the cost function to the standard QP format

MPC optimizes a cost function in order to determine its future input sequence. The cost function used in this thesis is shown in Eq. (33) and contains two terms: output error and input effort. The output error is the difference between the predicted output $\hat{y}_p(k+j)$ and the reference $r(k+j)$ at each timestep $j = 1 \dots N$, whereas the input effort is defined by how much the control input changes between each timestep.

$$J_{MPC}(\Delta u, k) = \sum_{j=1}^N ((\hat{y}_p(k+j) - r(k+j))^T (\hat{y}_p(k+j) - r(k+j))) + \sum_{j=0}^{N_c} ((\Delta u(k+j))^T \lambda^2 (\Delta u(k+j))) \quad (33)$$

However, this cost function must be rewritten in the standard Quadratic Programming (QP) form for the QP solver:

$$J(\Delta u, k) = \frac{1}{2} \Delta u^T H \Delta u + F^T \Delta u \quad (34)$$

Note that only terms featuring Δu are relevant, and constant terms can be omitted. The determined expression for the output predictions is:

$$\hat{y}_p = \bar{\mathbf{y}} + M(x(k) - \bar{x}) + \Phi_1 \Delta u + \Phi_2 \mathbf{u}(\mathbf{k} - 1) \quad (35)$$

Note that since the system is linearized at every controller interval the term $x(k) - \hat{x}$ is always 0. Substituting Eq. (35) in Eq. (33), and writing the equation in matrix notation using the matrices as defined in Eq. (14) gives:

$$J_{MPC}(\Delta u, k) = (\bar{\mathbf{y}} + \Phi_1 \Delta u + \Phi_2 \mathbf{u}(\mathbf{k} - 1) - \mathbf{r})^T (\bar{\mathbf{y}} + \Phi_1 \Delta u + \Phi_2 \mathbf{u}(\mathbf{k} - 1) - \mathbf{r}) + \Delta u^T \lambda^2 \Delta u \quad (36)$$

By gathering terms featuring Δu :

$$J_{MPC}(\Delta u, k) = \Delta u^T (\Phi_1^T \Phi_1 + \lambda^2) \Delta u + (-\mathbf{r}^T \Phi_1 + \bar{\mathbf{y}}^T \Phi_1 + \mathbf{u}(\mathbf{k} - 1)^T \Phi_2^T \Phi_1)^T \Delta u \quad (37)$$

Which can be translated into the standard QP form of Eq. (34) by selecting:

$$H = 2(\Phi_1^T \Phi_1 + \lambda^2) \quad (38)$$

$$F = -\mathbf{r}^T \Phi_1 + \bar{\mathbf{y}}^T \Phi_1 + \mathbf{u}(\mathbf{k} - 1)^T \Phi_2^T \Phi_1$$

APPENDIX C
FAMILIARIZATION STAGE TASKS

Using the denotation of Fig. 20 the familiarization tasks were, in order:

- Position the endpoint at A. Rotate the stick all the way left and back right using maximum input, while keeping the boom still.
- Position the endpoint at C. Rotate the boom all the way up and back down using maximum input, while keeping the stick still.
- Position the endpoint at A. Move the endpoint to B while tracking the horizontal line.
- Position the endpoint at C. Move the endpoint to E while tracking the vertical line.
- Position the endpoint at A. Move downwards and dig through the soil to see how the soil updates itself.
- Position the endpoint at D. Move to F while providing maximum input to the boom, and track the vertical line while providing *smooth, low frequent* stick inputs.
- Position the endpoint at D. Move to F while providing maximum input to the boom, and track the vertical line while providing *wild, high frequent* stick inputs.

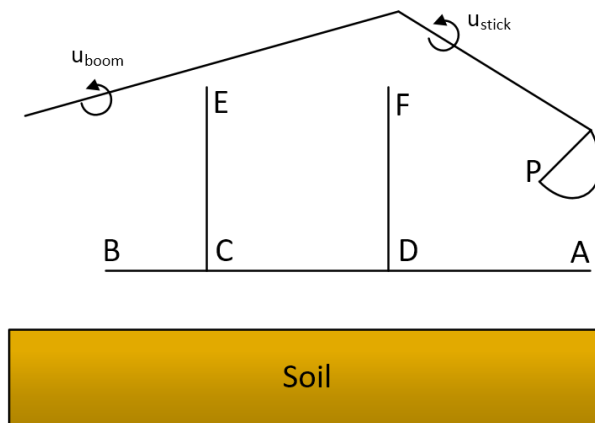
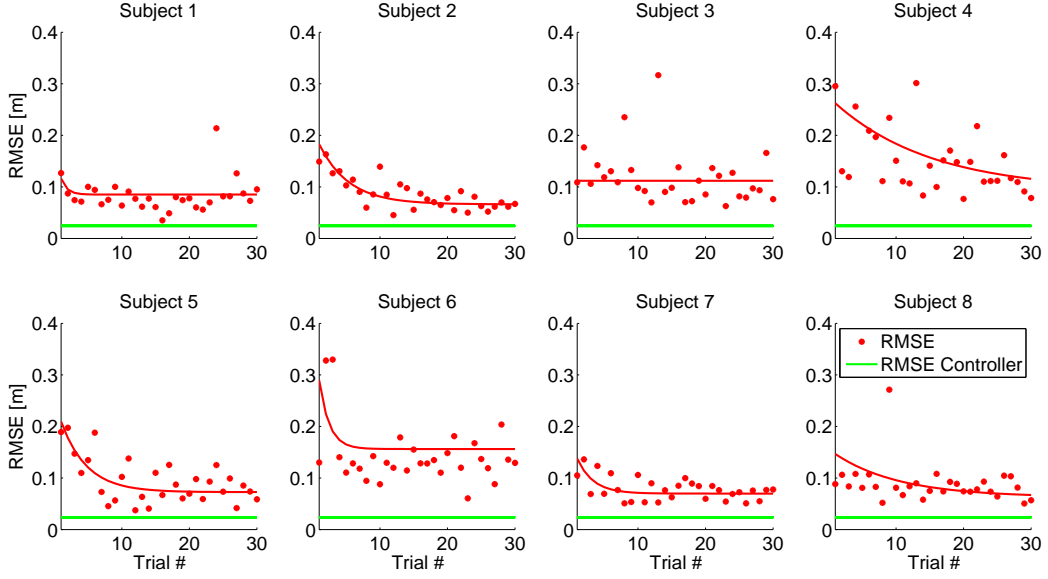
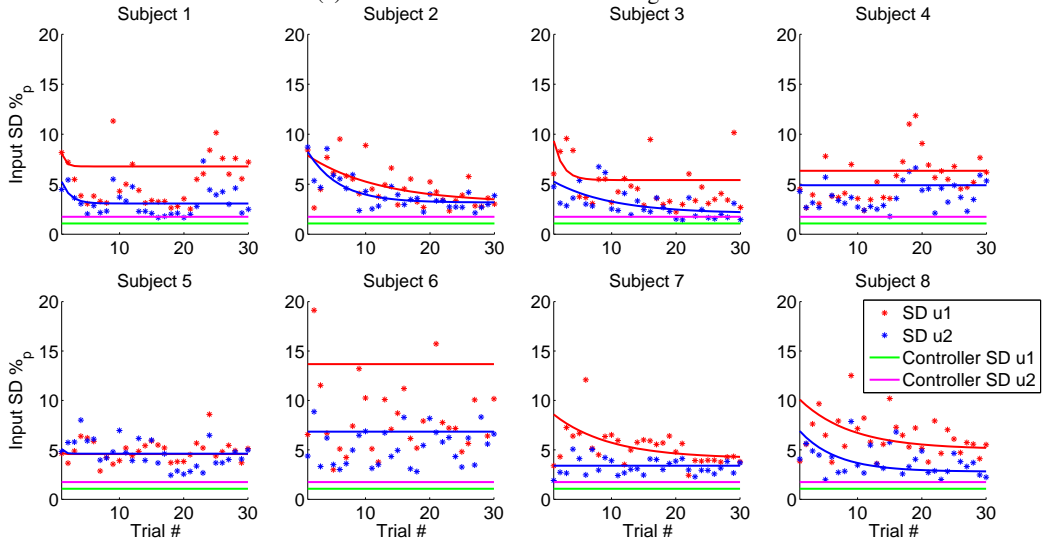


Fig. 20: Schematic drawing of the familiarization task. The point of interest in all tasks P is the endpoint of the bucket.

APPENDIX D
LEARNING CURVES



(a) RMSE for Task A with learning curves.



(b) Input SD for Task A with learning curves.

Fig. 21: Learning curves for the RMSE and input SD for task A. The learning curves were plotted by fitting an exponential function ([39]) of the form $RMSE(n) = \beta + \alpha e^{-\gamma n}$ where β is the final asymptotic performance, α is the initial performance, n is the trial number, and γ is the rate of learning. Values of the learning parameters and the quality of the fit are reported in Table V.

TABLE V: Learning parameters for task A.

RMSE				SD learning parameters				SD2			
α	β	γ	<i>Res</i>	SD1				α	β	γ	<i>Res</i>
0.0961	0.0851	1.1346	0.5857	0.0695	0.0678	1.6992	0.7071	0.0451	0.0307	0.7271	0.3140
0.1462	0.0661	0.2269	0.4200	0.0518	0.0313	0.0887	0.3538	0.0625	0.0317	0.2066	0.2343
0.1304	0.1118	9.7387	1.0103	0.0796	0.0542	0.7083	0.5834	0.0356	0.0207	0.1099	0.2780
0.1816	0.0930	0.0694	1.6882	0.0369	0.0634	8.4864	0.5993	0.0336	0.0490	7.2081	0.4485
0.1779	0.0726	0.2625	0.7602	0.0440	0.0458	3.9383	0.2571	0.0546	0.0462	2.4672	0.3406
0.2626	0.1562	0.6782	1.3565	0.1240	0.1367	17.7854	1.8804	0.0552	0.0684	15.0215	0.5958
0.1033	0.0698	0.4214	0.4928	0.0499	0.0413	0.1143	0.3509	0.0243	0.0339	13.4343	0.2105
0.0927	0.0630	0.1038	0.7353	0.0568	0.0507	0.1238	0.5100	0.0487	0.0280	0.1715	0.3473

APPENDIX E
DETERMINATION OF THE INPUT SMOOTHNESS METRIC SD AND THE PERFORMANCE METRIC RMSE

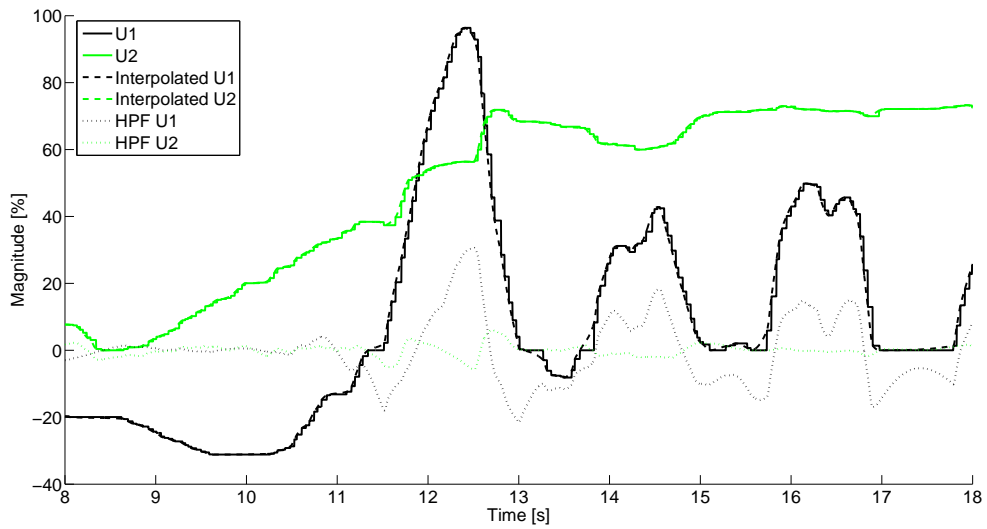


Fig. 22: Subject: determination of the input smoothness. The original input signal is first interpolated to remove discretization effects. Subsequently, a high pass filter with a cut-off frequency of 0.5 Hz was applied. Finally, the standard deviation of this remainder is taken.

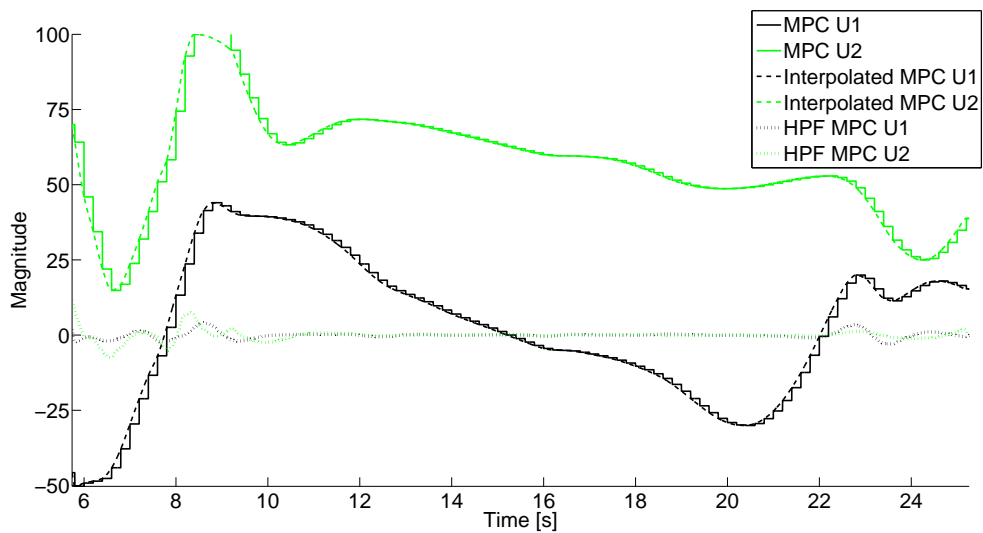


Fig. 23: MPC: Determination of the input smoothness. The original input signal is first interpolated to remove discretization effects. Subsequently, a high pass filter with a cut-off frequency of 0.5 Hz was applied.

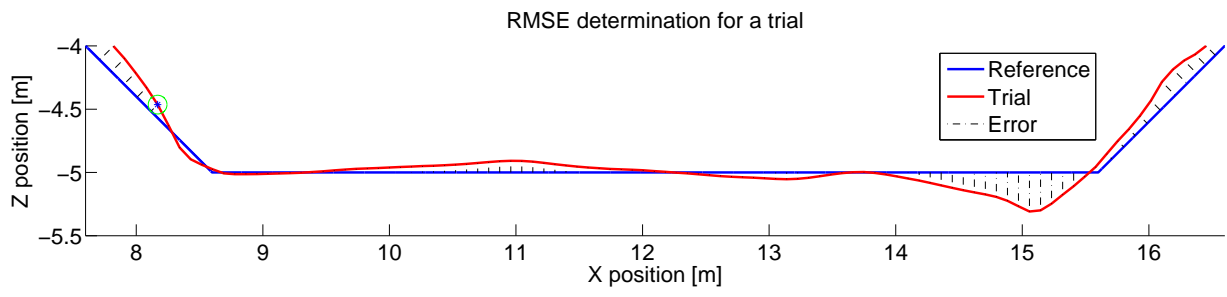
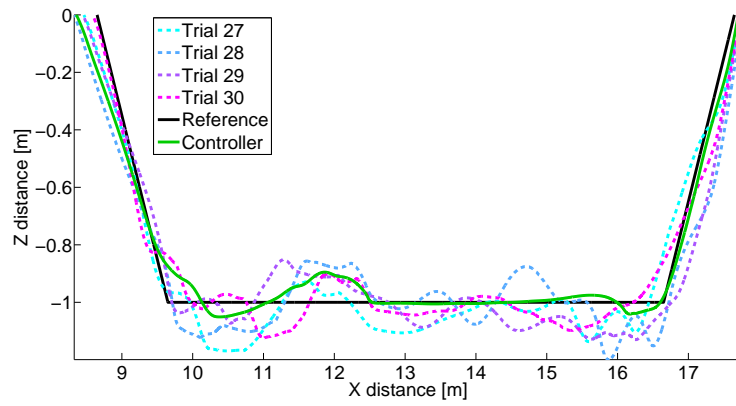
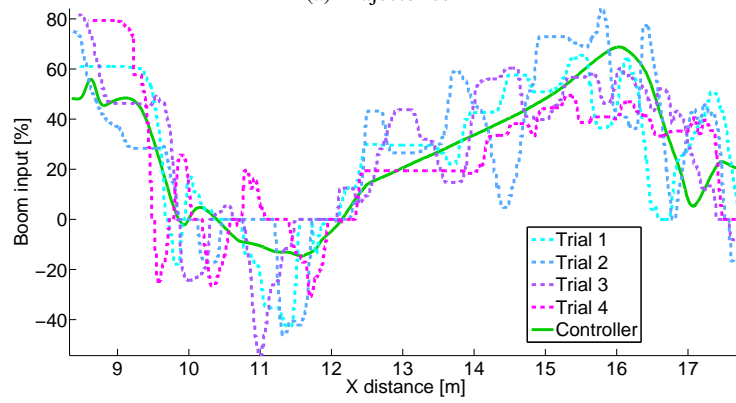


Fig. 24: RMSE determination for a trial. Visualization example with 100 points

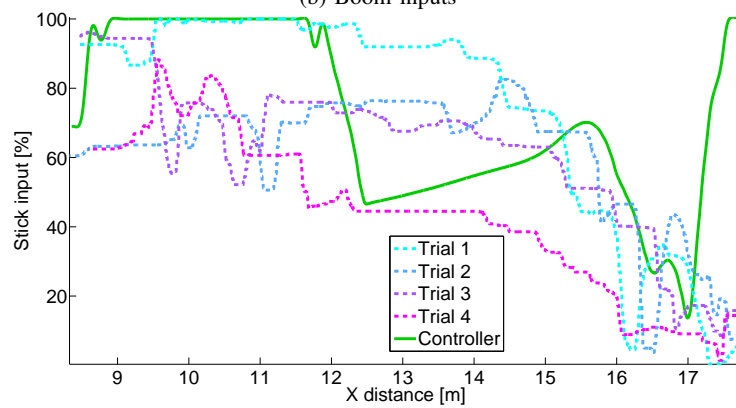
APPENDIX F
EXTRA FIGURES: COMPARISONS FOR TASK B1 AND B2, INPUT REVERSALS



(a) Trajectories

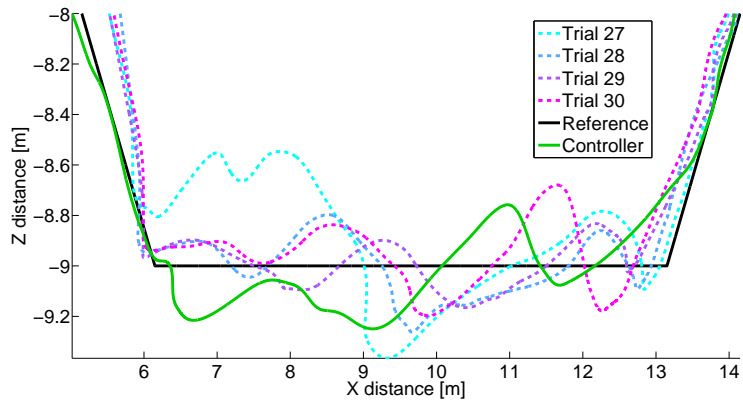


(b) Boom inputs

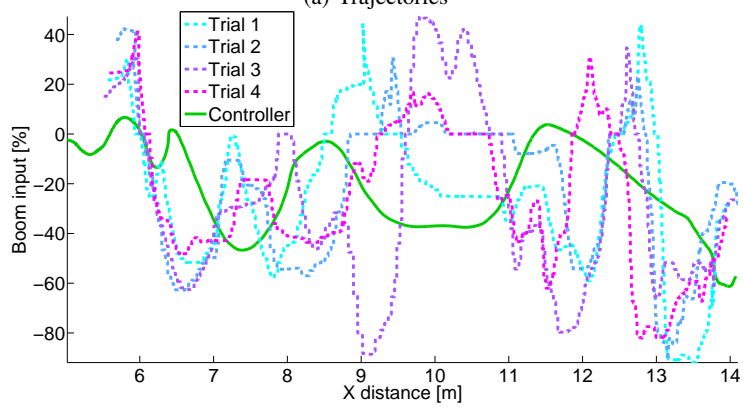


(c) Stick inputs

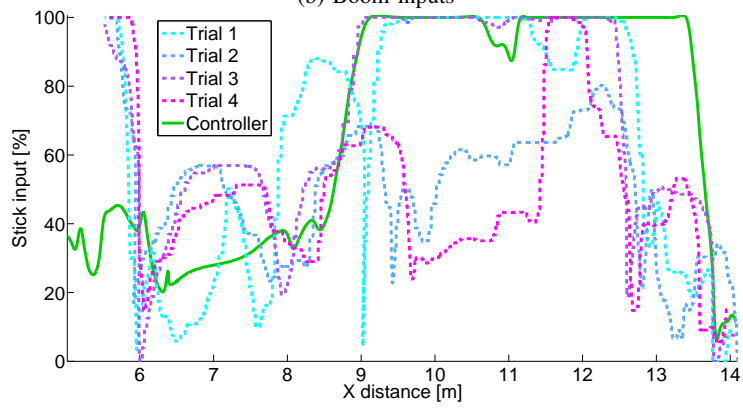
Fig. 25: Trajectories and control inputs of the last 4 trials of subject 7 in task B1 compared to the MPC. The three panels show the endpoint trajectories of the bucket (a) and the control inputs for the boom (b) and stick (c).



(a) Trajectories



(b) Boom inputs



(c) Stick inputs

Fig. 26: Trajectories and control inputs of the last 4 trials of subject 7 in task B2 compared to the MPC. The three panels show the endpoint trajectories of the bucket (a) and the control inputs for the boom (b) and stick (c).

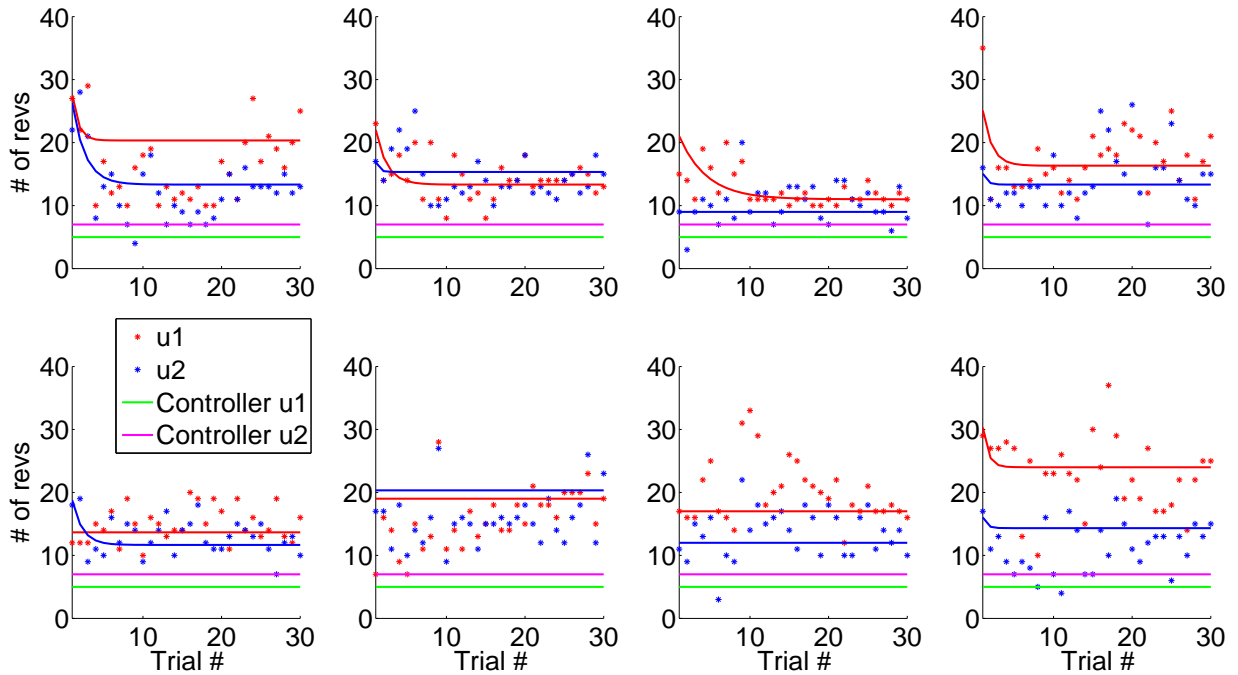


Fig. 27: Input reversals task A, for each subject and all trials. The learning curves were plotted by fitting an exponential function ([39]) of the form $RMSE(n) = \beta + \alpha e^{-\gamma n}$ where β is the final asymptotic performance, α is the initial performance, n is the trial number, and γ is the rate of learning.

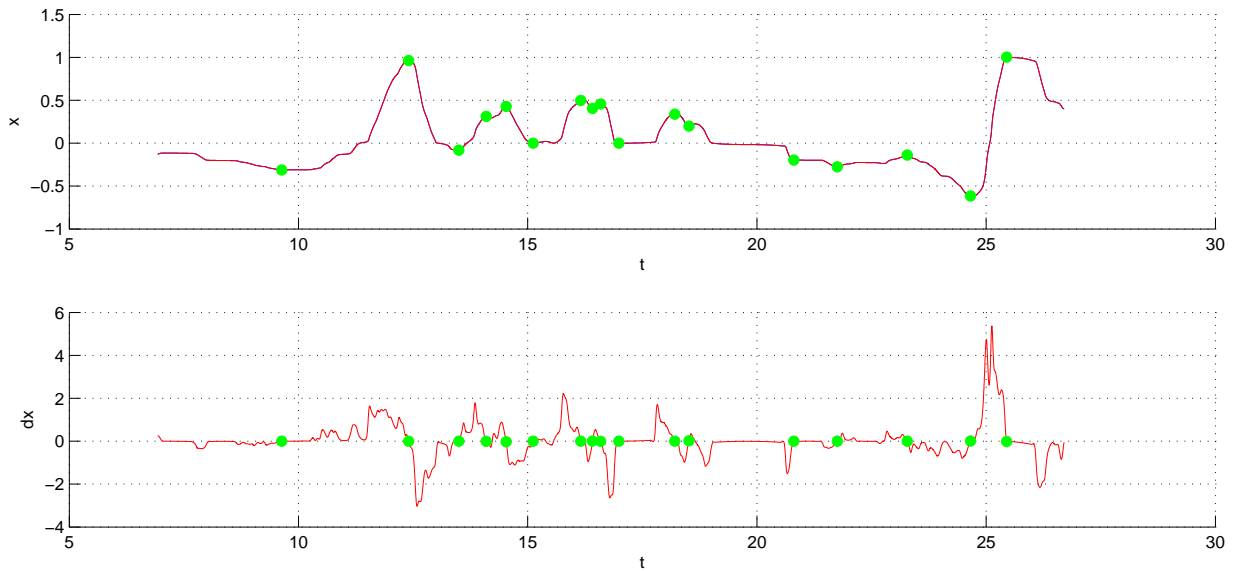


Fig. 28: Example of input reversal determination for one trial. An input signal (top plot) and its derivative (bottom plot) are shown. Each zero crossing of the derivative of the input signal is counted as one input reversal.

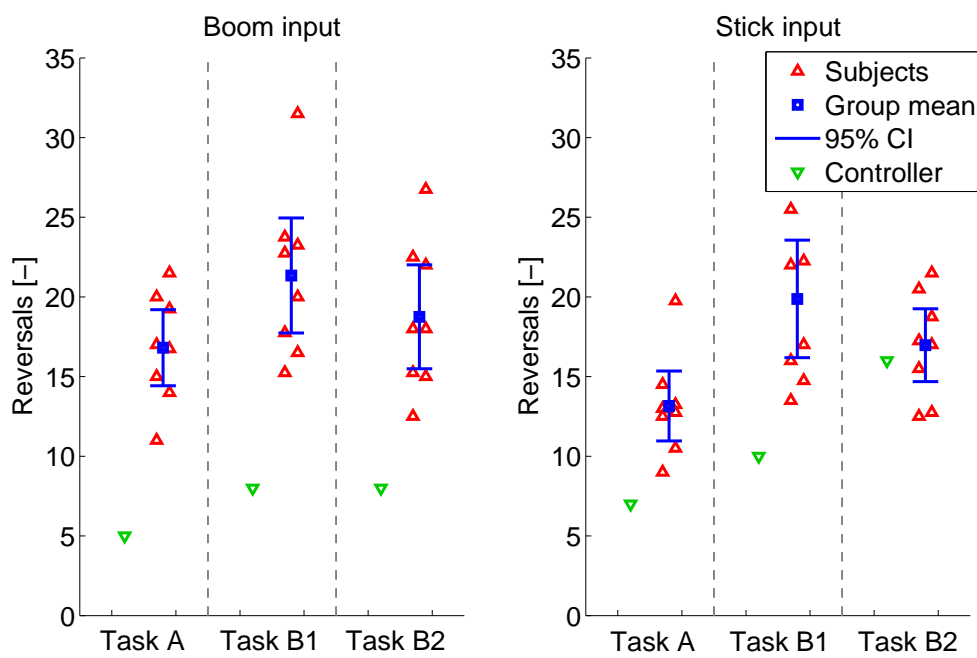
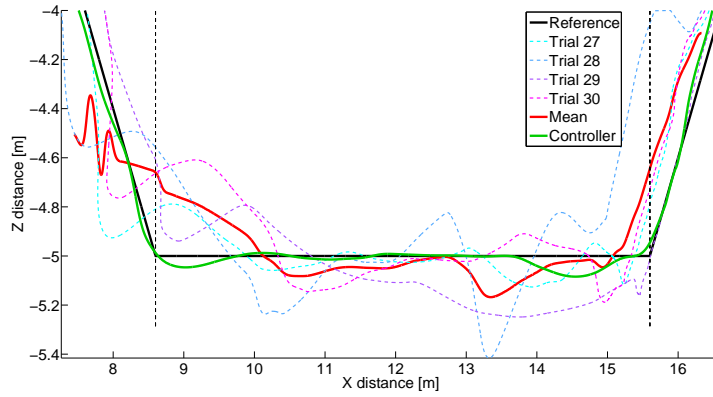
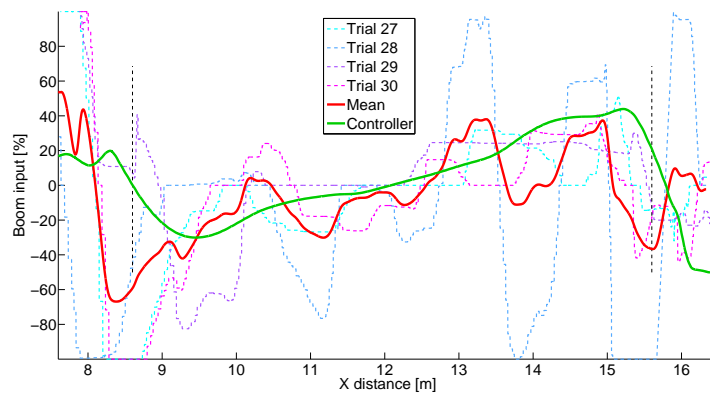


Fig. 29: Input reversals for both the controller and the subjects for the mean of the last 4 trials of all tasks.

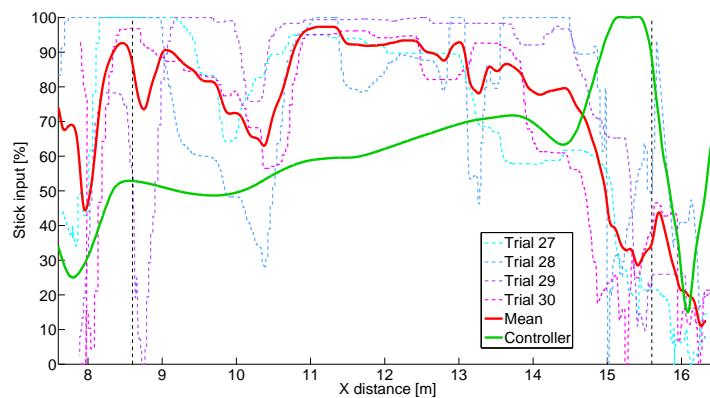
APPENDIX G
PERFORMANCE OF SUBJECT 6 FOR TASK A



(a) Endpoint trajectories of the bucket



(b) Control inputs for the boom



(c) Control inputs for the stick

Fig. 30: Trajectories and control inputs of the last 4 trials of subject 6 in task A. The subject exerted a large amount of bang-bang control, even after extended learning.

APPENDIX H
FREQUENCY RESPONSE PLOTS

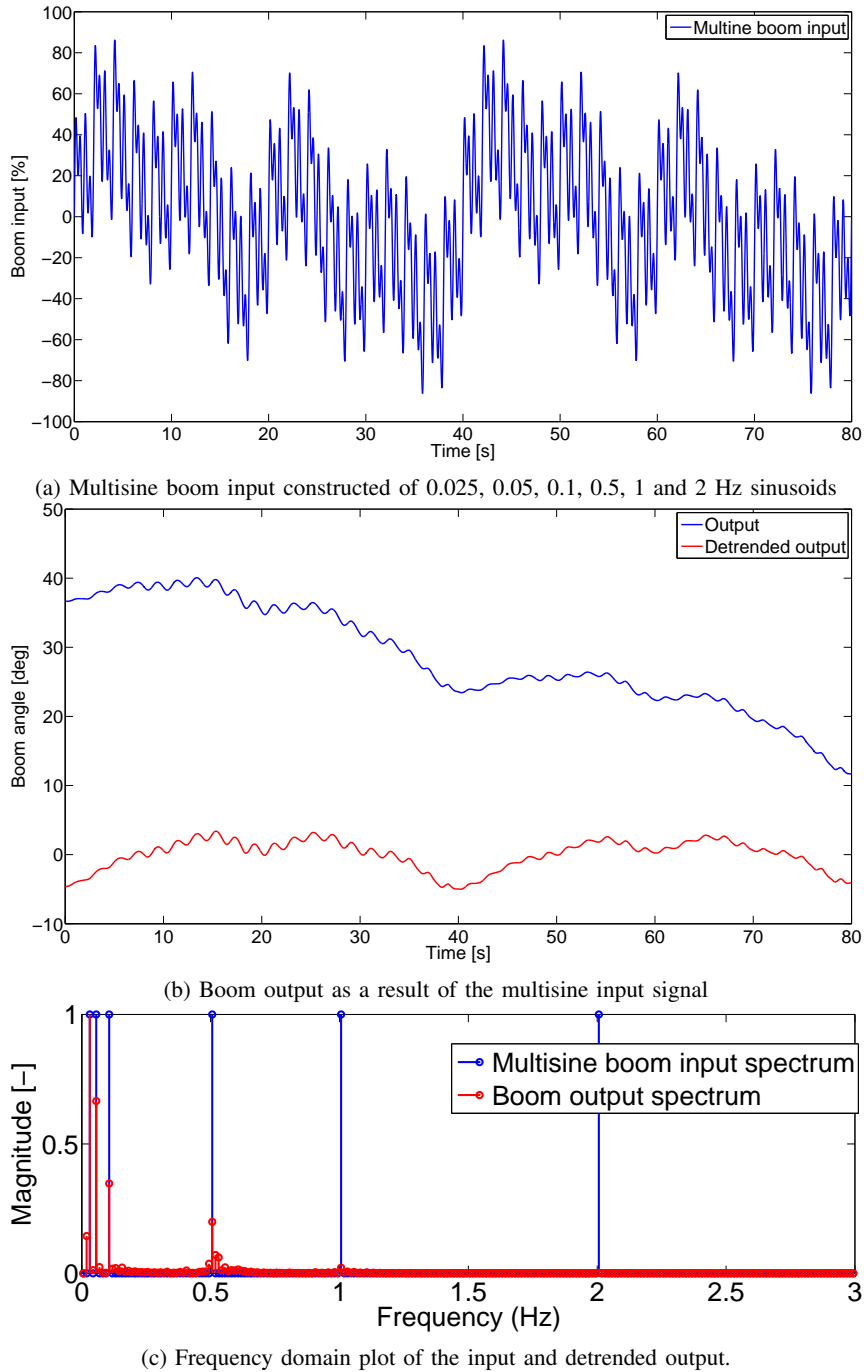


Fig. 31: A multisine input signal (a) was provided to the boom, resulting in the boom output (b). The signal was detrended to remove the influence of the up-down disparity. A frequency analysis of the input and output signals (c) shows that due to the slow dynamics low frequencies dominate.

APPENDIX I

Informed consent form for an offshore excavator digging simulator study.

Researchers:

Marco Stijnman - MSc. Student
E-mail: M.J.Stijnman@student.tudelft.nl
Tel: +31648549339

Ir. R.J. Kuiper - Supervisor
E-mail: r.j.kuiper@tudelft.nl

dr.ir. D.A. Abbink - Supervisor
E-mail: d.a.abbink@tudelft.nl

dr. ir. J.W. van Wingerden - Supervisor
E-mail: J.W.vanWingerden@tudelft.nl



Figure 1. Offshore excavator

Location:

TU Delft Faculty of Mechanical, Maritime and Materials Engineering
Haptics Lab 34 F-1-360
Mekelweg 2, 2628 CD Delft

This document provides information relevant for your participation in the digging simulator study. Please read this information thoroughly before starting the experiment. Note that at any time during the experiment you may ask for clarification of anything written here. Before each new task the relevant information will orally be repeated to you. You are also free to request a break at any point during the experiment.

Procedure:

In this experiment you will control an offshore excavator (see Figure 1). The visualization software (see Figure 3) used to display the excavator is identical to software actually used in the field. You will perform multiple digging trials with various conditions using a 2 D.o.F joystick (Figure 2). Note that you will not have to control the bucket, but will only manipulate the position of the boom and the stick. Please take a look at Figure 3, where the boom and the stick are indicated. Moving the joystick left moves the stick to the left and vice versa. Pulling the joystick *Towards* you will move the boom *Upwards* and pushing the joystick *Away* from you will move the boom *Downwards*. This seemingly counterintuitive movement comes from the fact that you would normally sit in the cabin, and pulling the joystick towards you corresponds to pulling the boom up, and pushing the joystick away pushes the boom away as well. Note that you will not be using end-point control here!.



Figure 2. Joystick

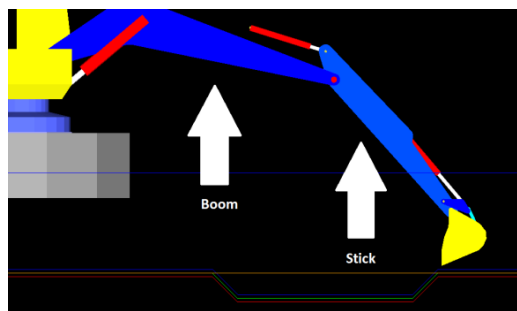


Figure 3. Visualization software

Firstly, there will be a familiarization task where we will do various small tasks to get you a feel of how the excavator moves. Note that in this trial the dynamics and soil forces of the excavator are turned off, which means that the excavator in subsequent parts of the experiment will feel a bit different. The set of small tasks to be performed will be listed upon the start of the familiarization task.

Afterwards, with all dynamics turned on, there is a set of 10+20 trials for the first condition. This condition will be the same for all 30 trials. In these first 10 trials performance is *not* important and enable you to get some training with the excavator and the task. For the 20 subsequent tasks performance *is* important.

Afterwards, you will perform a set of 17 more difficult tasks. In these tasks the position and type of soil changes between tasks. Before starting this task I will show you the different positions on the visualization software.

Task objective

Note that in all tasks the brown line corresponds to the soil. The green line is the desired trajectory of the bucket, which you should aim to follow as closely as possible while trying to stay within a time range of 20– 25 seconds as indicated by the timer on your screen. Try to perform the digging task in a smooth motion; avoid going backwards to correct any errors you made. Finally, all tasks are possible to finish.

Duration: The total experiment, including instructions, will take about an hour.

Risks or discomforts: None. If you feel unwell or uncomfortable in any way a pause can always be taken.

Confidentiality: Names are not recorded, and you will be assigned a subject number. Your data will be used for research purposes only.

Right to refuse or withdraw: You are free to stop the experiment at any time without having to provide an explanation.

I have read and understood the information provided above and hereby I give permission to process my data for this excavator experiment as described above. I voluntarily agree to participate in this study.

Name of participant:

Signature:

Date:

